

Non-Hermitian Topological Phases: Principles and Prospects

Ayan Banerjee,¹ Ronika Sarkar,^{2,1} Soumi Dey,¹ and Awadhesh Narayan^{1,*}

¹*Solid State and Structural Chemistry Unit,*

Indian Institute of Science, Bangalore 560012, India

²*Department of Physics, Indian Institute of Science, Bangalore 560012, India*

(Dated: December 21, 2022)

Abstract

The synergy between non-Hermitian concepts and topological ideas have led to very fruitful activity in the recent years. Their interplay has resulted in a wide variety of new non-Hermitian topological phenomena being discovered. In this review, we present the key principles underpinning the topological features of non-Hermitian phases. Using paradigmatic models – Hatano-Helson, non-Hermitian Su-Schrieffer-Heeger and non-Hermitian Chern insulator – we illustrate the central features of non-Hermitian topological systems, including exceptional points, complex energy gaps and non-Hermitian symmetry classification. We discuss the non-Hermitian skin effect and the notion of the generalized Brillouin zone, which allows restoring the bulk-boundary correspondence. Using concrete examples, we examine the role of disorder, present the linear response framework, and analyze the Hall transport properties of non-Hermitian topological systems. We also survey the rapidly growing experimental advances in this field. Finally, we end by highlighting possible directions which, in our view, may be promising for explorations in the near future.

* awadhesh@iisc.ac.in

CONTENTS

I. Introduction	3
II. Exceptional Points	4
III. Paradigmatic Models	10
A. Hatano-Nelson Model	10
B. Non-Hermitian Su-Schrieffer-Heeger Model	12
C. Non-Hermitian Chern Insulators	16
D. Non-Hermitian Topological Semimetals	18
IV. Non-Hermitian Symmetry Classes	21
V. Complex Energy Gaps in non-Hermitian systems	23
VI. Non-Hermitian Skin Effect	25
VII. Broken Bulk-Boundary Correspondence and the Generalized Brillouin Zone	26
VIII. Disorder Effects in Non-Hermitian Systems	29
IX. Non-Hermitian linear response theory	32
X. Transport signatures of non-Hermitian systems	35
XI. Physical Platforms and Experimental Advances	37
XII. Overview and Outlook	40
Acknowledgments	41
References	41

I. INTRODUCTION

Hermiticity is a central pillar of quantum mechanics, which dictates that the observables be represented by Hermitian or self-adjoint operators [1]. It leads to conservation of probability and real eigenvalues of such operators. However, since the early days of quantum mechanics it was noted that many systems exhibit a lack of probability conservation due to exchange of particles or energy with their surroundings [2]. In the recent decades, pioneering work by Bender and co-workers radically transformed the understanding of non-Hermitian Hamiltonians [3, 4]. This field has today burgeoned into the exciting forefront of non-Hermitian systems. Interestingly, not only quantum, but also a variety of classical systems can be non-Hermitian in nature. It has been realized that non-Hermitian systems exhibit many properties that are unique to them and do not have any analogs in Hermitian systems.

The last decades have witnessed a growing interest in ideas from topology in physics, beginning with the quantum Hall effect [5]. Remarkable connections to topology have culminated in the celebrated topological band theory, which is at play in topological insulators, topological semimetals, and topological superconductors [6–9]. A cornerstone in the analysis of topological phases has been the bulk-boundary correspondence – bulk topology is reflected in the existence of symmetry-protected boundary states. Often such topological phases also harbor protected band crossings, which lead to exotic experimental signatures. Moreover, an astonishing range of experimental platforms have been recognized to host these exciting phenomena, ranging from condensed matter materials [10], ultra-cold atoms [11, 12], photonic [13, 14] and phononic [15] systems, to name just a few.

In recent years, the synergy between non-Hermitian concepts and topological ideas has led to extremely fruitful and rapid activity. Their union has resulted in a wide variety of new non-Hermitian phenomena being discovered and reinterpreted within the framework of topology. We note here that there are several excellent reviews on complementary aspects of non-Hermitian systems [16–22]. In this review, we focus on the key concepts and ideas underpinning topological features of non-Hermitian systems, and summarize the latest developments in this fast evolving field. We start with a discussion of exceptional points, which are ubiquitous in non-Hermitian topological phases and can be thought of as an intriguing generalization of Hermitian band degeneracies. We next present paradigmatic

models which have played a vital role as playgrounds for discovering many of the salient features of non-Hermitian topological phases. These include the Hatano-Nelson and non-Hermitian Su-Schrieffer-Heeger models in one dimension, the non-Hermitian Chern insulator model in two dimensions and non-Hermitian topological semimetals in three dimensions. We thoroughly discuss their spectral topology and use them to illustrate many of the important features of non-Hermitian topological systems. We then present a detailed discussion of the non-Hermitian symmetry classes which generalize the celebrated Altland-Zirnbauer classification of Hermitian systems. We illustrate the ideas using the non-Hermitian Su-Schrieffer-Heeger model. We then discuss the notion of complex energy gaps and how they lead to intrinsically non-Hermitian phenomena. Next, we present the non-Hermitian skin effect, which is completely unique to non-Hermitian systems. We subsequently highlight the broken bulk-boundary correspondence in non-Hermitian topological phases and how the role of a generalized Brillouin zone becomes crucial, using the non-Hermitian Su-Schrieffer-Heeger model as a concrete example. The role of disorder and its interplay with symmetries in non-Hermitian systems is next summarized. In particular, we highlight the intriguing phenomenon of non-Hermitian Anderson skin effect. The linear response theory is widely used for characterizing the response of any system under the influence of an external perturbation. In this regard, a framework of non-Hermitian linear response has been recently proposed, which we present. We further analyze the transport signatures in the non-Hermitian Chern insulator as a concrete example of the theory. We next survey the numerous experimental advances made in the field. Finally, we end with an outlook on the possible upcoming new directions in this rapidly developing field.

II. EXCEPTIONAL POINTS

One of the most striking feature of non-Hermitian systems is the presence of non-Hermitian degeneracies called exceptional points (EPs) [23]. These EPs are spectral singularities in the parameter space (which is in general complex) of the Hamiltonian where both the eigenvalues and the eigenvectors coalesce. This is unlike Hermitian degeneracies where the eigenmodes become orthogonal at a Dirac point [6]. We start with a simple two-level system that reveals the intricate structures of EPs illustratively. Consider the Hamiltonian matrix,

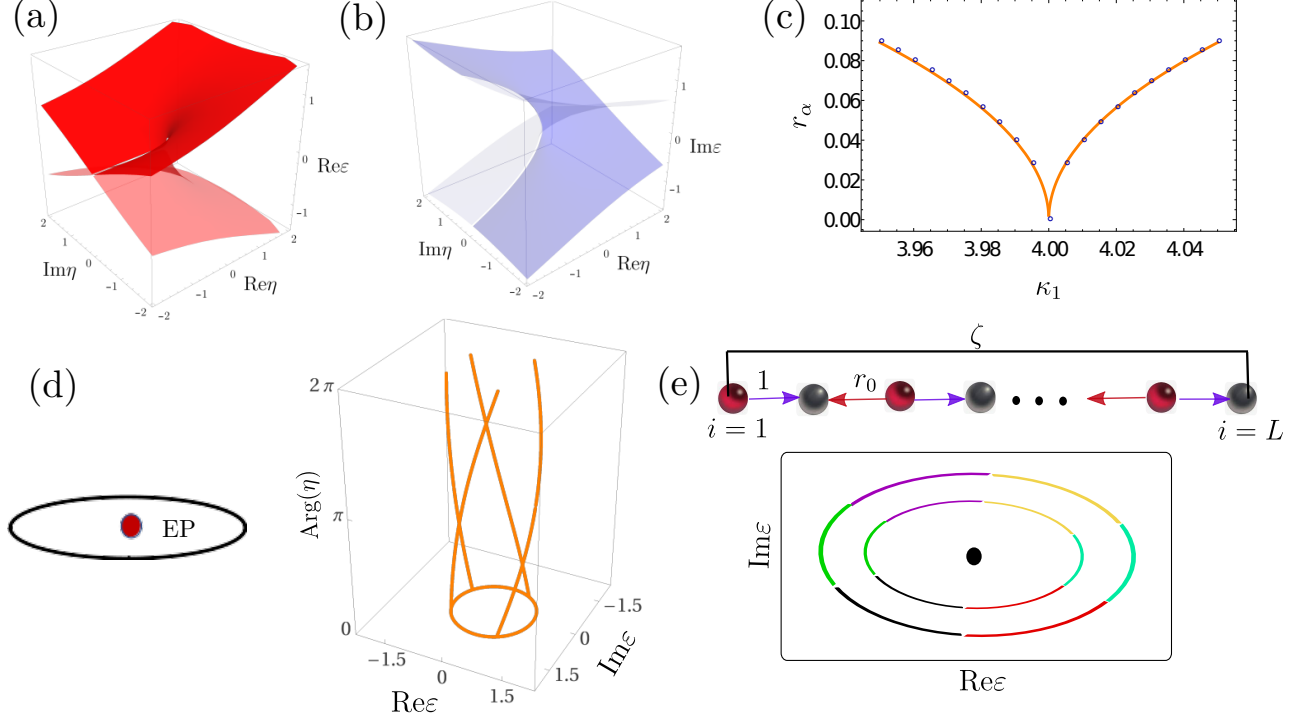


FIG. 1. **Characterization and topological features of exceptional points.** Perspective view of (a) real and (b) imaginary energy exhibiting Riemann sheet structure of two coalescing energy levels in the complex η -plane. (c) Phase rigidity for diagnosing EPs in the parameter space showing square root scaling around the EP. (d) Eigenvalue switching manifests the Riemann sheet topology while encircling a fourth-order EP by tuning the system parameters. (e) Top panel is a schematic describing the model in Eq. 9. The bottom panel is a schematic of eigenvalue spectra in different colors showing how the eigenvalues vary with ϕ in the complex plane for different values of ζ . The six colors in the spectrum represent three unit cells. As long as $\zeta \neq 0$, one needs three rounds of ϕ to return to the initial eigenvalue sheet. Here $\zeta = 0$ is a higher-order EP, where all eigenstates coalesce.

$$H = \begin{pmatrix} \epsilon_1 & \kappa_1 \\ \kappa_2 & \epsilon_2 \end{pmatrix}. \quad (1)$$

Note that this Hamiltonian describing this two-level system is non-Hermitian ($H^\dagger \neq H$) since $\kappa_1 \neq \kappa_2^*$, in general. The energy eigenvalues can be written as $\varepsilon_\pm = E_0 \pm \sqrt{\eta}$, where $E_0 = \frac{\epsilon_1 + \epsilon_2}{2}$ and $\eta = \frac{(\epsilon_1 - \epsilon_2)^2}{4} + \kappa_1 \kappa_2$. In general all parameters $\epsilon_1, \epsilon_2, \kappa_1$ and κ_2 can be complex. Interestingly, $\eta = 0$ is a degeneracy point. We will see how this goes beyond a

usual Hermitian degeneracy (see Fig. 1(a)). At this special point, we investigate the nature of eigenmodes. We will invoke the notion of bi-orthogonal basis consisting of both left and right eigenvectors [24]. Let $|\psi^R\rangle$ and $\langle\psi^L|$ be the right and left eigenvectors of H with the same eigenvalue ε_i such that as long as $\varepsilon_i \neq \varepsilon_j$, they become bi-orthogonal $\langle\psi^L|\psi^R\rangle = 0$. We have

$$H|\psi^R\rangle = \varepsilon_i|\psi^R\rangle, \quad \langle\psi^L|H = \varepsilon_i\langle\psi^L|. \quad (2)$$

The right and left eigenvectors of the system read

$$|\psi^R\rangle = \begin{pmatrix} \frac{(\epsilon_1 - \epsilon_2)}{2\kappa_2} \pm \frac{\sqrt{\eta}}{\kappa_2} \\ 1 \end{pmatrix}, \quad \langle\psi^L| = \left(\frac{(\epsilon_1 - \epsilon_2)}{2\kappa_1} \pm \frac{\sqrt{\eta}}{\kappa_1} \quad 1 \right). \quad (3)$$

Strikingly, at the degeneracy point $\eta = 0$ both the right eigenvectors and left eigenvectors coalesce. Consequently, the eigenvectors do not span the full Hilbert space and the system becomes defective – this is the key signature of an EP. The right and left eigenvectors are orthogonal to each other at the EP. There exists a quantitative measure of eigenfunctions' biorthogonality. It is the phase rigidity, which is an experimentally measurable quantity. The phase rigidity, r_α , is defined as [25, 26],

$$r_\alpha = \frac{\langle\psi_\alpha^L|\psi_\alpha^R\rangle}{\langle\psi_\alpha^R|\psi_\alpha^R\rangle}, \quad (4)$$

where ψ_α^L and ψ_α^R are the biorthogonal left and right eigenvectors of a state α . On approaching the EP ($\eta \rightarrow 0$), right and left eigenvectors align and the phase rigidity vanishes ($r_\alpha \rightarrow 0$) (see Fig. 1(c)). In contrast, $r_\alpha = 1$ for a Hermitian system. In summary, EPs are a special kind of non-Hermitian degeneracy in the complex parameter space of the Hamiltonian where two or more eigenstates coalesce and the spectrum collapses to a single eigenvalue showing spectral singularities. Mathematically, the algebraic multiplicity (degenerate eigenvalues) exceeds the geometric multiplicity (number of independent eigenvectors) with an incomplete set of eigenfunctions, rendering the Hamiltonian defective, a situation that is truly unique to non-Hermitian system [27]. In general, a Hamiltonian with dimension m being non-diagonalizable at the EP with energy ε_0 , can be brought to a Jordan block form of order m . The system still has m degenerate eigenvalues, but there exists only one eigenvector [28].

The crucial distinction between the Hermitian and exceptional degeneracies can be effectively captured by rewriting our Hamiltonian in the following generic form [20]

$$H(\delta) = \mathbf{f}(\delta) \cdot \sigma, \quad (5)$$

where $\mathbf{f} = \mathbf{f}_R + i\mathbf{f}_I$ with $f_R, f_I \in \mathbb{R}^3$ and the Pauli matrices form the basis of two dimensional matrices and represent the pseudo spin degrees of freedom. The energy eigenvalues read $\varepsilon = \sqrt{f_R^2 - f_I^2 + 2i\mathbf{f}_R \cdot \mathbf{f}_I}$. The Hermitian degeneracies occur with the condition that $\mathbf{f}_R = 0$ which can be tuned by the parameters of spatial dimension in an n -dimensional system which will typically be a point. For the present case, the Hermitian degeneracy occurs only if both $\epsilon_1 = \epsilon_2$ and $\kappa_1 = \kappa_2^* = 0$ – the resulting degeneracy has co-dimension 3. Whereas, for the non-Hermitian case \mathbf{f}_I is in general non-zero. The occurrence of non-Hermitian degeneracies leads to the following conditions –

$$f_R^2 - f_I^2 = 0 \quad \text{and} \quad \mathbf{f}_R \cdot \mathbf{f}_I = 0, \quad (6)$$

with the tuning of two spatial dimensions. One may also encounters trivial degeneracies, also known as diabolic points, with both $\mathbf{f}_R = \mathbf{f}_I = 0$. These lack the information regarding coalescence of eigenfunctions [29].

It is interesting to note that exceptional contours (ECs) can also appear in a non-Hermitian system. These are comprised entirely of EPs, where phase rigidity vanishes over a surface instead of a single point [30]. The general criteria for obtaining an EC are the following

$$\begin{aligned} \text{Re det}[H(\delta)] &= 0, \\ \text{Im det}[H(\delta)] &= 0. \end{aligned} \quad (7)$$

These two constraint equations in a higher dimensional system allow to form EC where both the eigenvectors and eigenvalues merge without any additional symmetry. These ECs preserve quantized topological charges [31, 32].

Very recently, the role of higher-order EPs (HEPs) has come to the forefront in the context of enhanced response even with amplified perturbation [33]. To better understand HEPs, let us consider a system described by a Hamiltonian H_0 subjected to a small perturbation

λH_1 in the vicinity of the EP. The eigenenergies of the combined system, $H(\lambda) = H_0 + \lambda H_1$, can be expressed as a power series in λ in the neighborhood of the EP [23, 34].

$$\varepsilon_h = \varepsilon + \alpha_1 \omega^h \lambda^{1/p} + \alpha_2 \omega^{2h} \lambda^{2/p} + \dots, \quad (8)$$

where $h = 0, 1, \dots, p-1$, $\omega = \exp(2\pi/p)$, $\alpha_1 = (\langle \psi_L | H'(0) | \psi_R \rangle)^{1/m}$, and $H'(0) = \frac{\partial H(\lambda)}{\partial \lambda}|_{\lambda=0}$ and p is the dimension of the system. Such an expansion shows that $|\varepsilon_h(\lambda) - \varepsilon|$ is in general of the order of $|\lambda|^{1/p}$ for small λ . This immediately suggests that the first-order response of a non-Hermitian system varies as $|\lambda|^{1/p}$ around an EP. Therefore the system in non-Hermitian setting provides better sensitivity in sensors than the system in a Hermitian one, where the first-order response is expected to vary linearly in λ [31]. Since a p -th order EP requires coalescing of p levels and results in a sudden reduction in dimensionality in the system, typically, there should be $2(p-1)$ real constraints needed to detect it in systems without any symmetry. However, recent pioneering studies reveal that symmetry can substantially reduce the number of constraints [35–37].

We note that Eq. 8 reveals delicate topological behaviour around an EP. For instance, the fractional exponent in Eq. 8 suggests that the different eigenmodes intersect each other due to the underlying Riemann sheet topology when enclosing an EP by tuning the system parameters. Specifically, if we encircle an EP (without intersecting it) with a closed loop S , then the eigenvalues can be expressed as a set of p holomorphic functions such as $\{\varepsilon_1(\lambda), \varepsilon_2(\lambda), \dots, \varepsilon_p(\lambda)\}$ (see Fig. 1(d)). Now if S is rotated continuously around $\lambda = 0$, these p functions can be continued analytically [23, 34, 38]. They would have undergone a permutation among themselves upon one revolution of S . For instance, in our case of Eq. 1, we consider a small perturbation away from the EP ($\eta = 0$) by a complex number ($\eta = \Delta e^{i\phi}$, where $\Delta, \phi \in \mathbb{R}$) in the parameter space. When we tune ϕ from 0 to 2π to encircle the EP in the parameter space, the two eigenvalues get exchanged around the EP – $\{E_0 + \sqrt{\eta}, E_0 - \sqrt{\eta}\} \rightarrow \{E_0 - \sqrt{\eta}, E_0 + \sqrt{\eta}\}$ (see Fig. 1(a)). This exchange behavior has been geometrically interpreted in terms of the holonomy matrix [39]. The intricate topological structure in the neighbourhood of multiple EPs leads to interesting consequences [40]. The topological nature stems from the fact that these rich non-trivial scenarios do not depend on the precise shape of the loop as long as it encloses the EP.

We next delve into the emergence of the topological properties arising from the appearance

of EPs while transitioning from periodic boundary conditions (PBC) to open boundary conditions (OBC) through the tuning of a twisted boundary condition. To analyze this we adapt the following model from Ref. [41] by choosing $\epsilon_1 = \epsilon_2 = 0$, $\kappa_1 = 1$ and $\kappa_2 = r_0 e^{-ik}$, such that Eq. 1 becomes

$$H = \begin{pmatrix} 0 & 1 \\ r_0 e^{-ik} & 0 \end{pmatrix}. \quad (9)$$

This model gives rise to an EP at $r_0 = 0$, and the swapping of eigenvalues can be observed around the EP by tuning k from 0 to 2π . Next, we go to the real space version of this model after a Fourier transformation, where r_0 describes the unidirectional inter-unit cell hopping and unity on the right corner in Eq. 9 represents the unidirectional intra-cell hopping in the unit cell comprising of two inequivalent atoms, as depicted in Fig. 1(d). Furthermore, we modulate the boundary condition with a twisted coupling between the first and the last sites. The system Hamiltonian in real space representation takes the following form

$$H = \sum_{i=1}^L c_{i,A}^\dagger c_{i,B} + r_0 c_{i+1,A}^\dagger c_{i,B} + \zeta e^{i\phi} c_{L,B}^\dagger c_{1,A}, \quad (10)$$

where $c_{i,\alpha}^\dagger (c_{i,\alpha})$ is the fermionic creation (annihilation) operator at site i for sublattice $\alpha = A, B$ (see Fig. 1(d)). Here L is the total number of sites. The last term specifies the twisted hopping between two ends. $\zeta = 0$ corresponds to OBC. Whereas with $\zeta = r_0$ and $\phi = 0$ the translation symmetry is restored and the eigenvalues read $\varepsilon = r_0 e^{ik/2}$ with L discrete k points. Here, ϕ connects the wavevectors through a gauge transformation – it transforms all the related phases between inter unit cells to a total phase jump $e^{i\phi} = e^{iLk}$ across the two ends [42]. One can tune ϕ from 0 to 2π in Eq. 10 to observe eigenmodes switching among L eigenvalues in the complex plane (see Fig. 1(d)). Now, if we modulate the boundary condition with $\zeta = \Theta r_0$ and unless Θ approaches to zero the translational symmetry can still be maintained with a renormalized hopping. Consequently, the swapping of eigenvalues in a complex loop can still be observed (see Fig. 1(d)). Strikingly, at $\Theta = 0$ we are right at an EP under OBC and all the eigenstates coalesce to a *single* point in the spectrum. Consequently, the eigenspectrum changes dramatically while tuning from PBC to OBC. Thus, the connection between bulk topological invariant in PBC and the presence of topological boundary modes becomes elusive and leads to violation of celebrated bulk

boundary correspondence [20, 41], which we will discuss in more detail shortly. The interplay between the role of higher-order EPs, extreme sensitivity in boundary conditions, and the occurrence of bulk-boundary correspondence is a very active topic of current research [16, 21, 43].

III. PARADIGMATIC MODELS

Next, we discuss key models which have been instrumental in the development of topological ideas in the context of non-Hermitian systems – the Hatano-Nelson model, the non-Hermitian Su-Schrieffer-Heeger model, the non-Hermitian Chern insulator model, and non-Hermitian topological semimetal models. In the following we present the interesting spectral topology and topological band properties of each of these systems, which serve as the foundation for the following discussions.

A. Hatano-Nelson Model

We start with the Hatano-Nelson model, a prototypical one band non-Hermitian model with non-reciprocal hopping in a one-dimensional geometry, which was originally proposed to study localization and vortex pinning in disordered type II superconductors [44, 45]. The non-interacting Hatano-Nelson model has the Hamiltonian

$$H = \sum_j (J_L c_j^\dagger c_{j+1} + J_R c_{j+1}^\dagger c_j), \quad (11)$$

where $J_R, J_L \in \mathbb{R}$ introduce the hopping asymmetry in the lattice leading to the non-Hermiticity (see Fig. 2(a)). Moving to the k -space by Fourier transforming the operators (using $c_j = \sum_k c_k e^{ikj}$), we obtain the momentum space Hamiltonian, $H_k = (J_R + J_L) \cos k + i(J_R - J_L) \sin k$. The dispersion is an ellipse in the complex plane with symmetric real energy and asymmetric imaginary energy parts, stipulating the non-reciprocal nature of the system. The eigenbands parameterized by k wind around the origin in anticlockwise (clockwise) for positive (negative) $J_L - J_R$. The different winding in the two cases can be described by spectral winding number ω ,

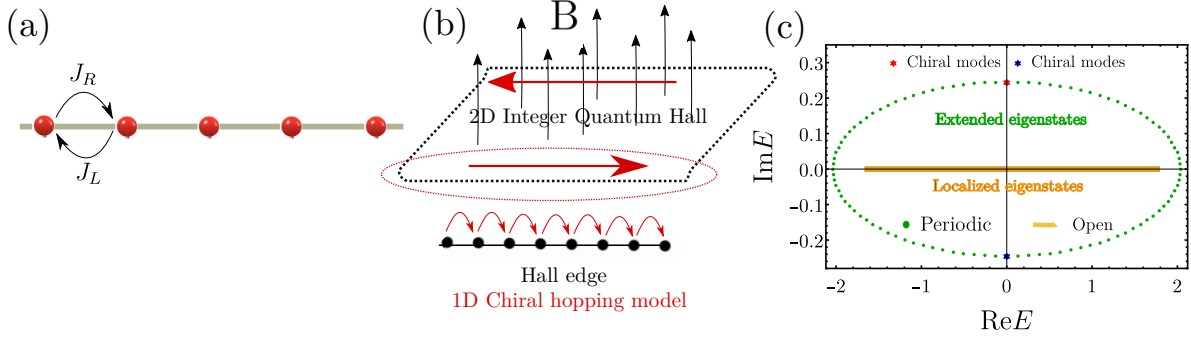


FIG. 2. **Hatano-Nelson model.** Schematic illustration of the Hatano-Nelson model (see Hamiltonian in Eq. 11). (b) The one-dimensional system characterized by an integer winding number in the chiral hopping model corresponds to the boundary of a two-dimensional system characterized by an integer quantum Hall state with a quantized Chern number. (c) The dispersion of the model in the complex plane under periodic and open boundary conditions. The chiral modes are also indicated, along with extended and localized eigenstates.

$$\omega = \int_{-\pi}^{\pi} \frac{dk}{2\pi i} \partial_k \ln(E_k - E_B), \quad (12)$$

which is nothing but the number of times the complex eigenband encloses the base point with energy E_B . The winding number reads

$$\begin{aligned} \omega &= 1 \quad \text{for } |J_L| > |J_R|, \\ &= -1 \quad \text{for } |J_L| < |J_R|. \end{aligned} \quad (13)$$

Here $J_L = J_R$ is a topological phase transition point. This structure of winding number suggests that the system exhibits a point gap around the origin ($E_B = 0$), which we will discuss in more detail. We note that in a remarkable recent study it has been shown that the Hatano-Nelson model corresponds to the edge of a two-dimensional system characterized by an integer quantum Hall state with a Chern number under appropriate time dynamics (see Fig. 2(b)) [46, 47]. Interestingly, this insight has led to the understanding that the winding numbers have a close correspondence with the chiral modes. The single particle current can be determined by the group velocity $\left(\propto \frac{\partial \text{Re}[E_k]}{\partial k}\right)$ and a lifetime given by the inverse of the imaginary part of the energy eigenvalue [46]. The left (right) propagating wave contributing to the chiral current depends on the sign of the positive (negative) imaginary energy. In

general, the one-to-one correspondence between winding number and chiral modes can be found as follows

$$\omega = \frac{1}{2} \sum_{n\alpha} \text{sign}[\text{Im}(E_n(k_{n\alpha}))] \text{sign}[\partial_k \text{Re}(E_n(k_{n\alpha}))], \quad (14)$$

where $\{k_{n\alpha} : \text{Re}(E_n(k_{n\alpha})) = 0\}$, i.e., $k_{n\alpha}$ are the wavevectors set where the real part of the energy vanishes, and α labels the number of such connected points in the spectrum. Here n denotes the band index. Thus, the topological winding number of the complex spectrum counts the number of chiral modes with $\text{Re}(E_n(k_{n\alpha})) = 0$. For instance, in case of the Hatano-Nelson model, the winding number corresponds to the difference between left-propagating modes minus the number of right-propagating modes for $k = \pi/2$.

Strikingly, another unique feature of this non-Hermitian model is the extreme sensitivity to the boundary conditions. The spectrum having completely real dispersion under OBC drastically changes under PBC where we find a complex spectrum in general (see Fig. 2(c)). Interestingly, the nature of eigenstates also changes radically since, under PBC, we get extended eigenstates. In contrast, the eigenstates become localized with an exponential amplitude profile in OBC, leading to the non-Hermitian skin effect. Consequently, under OBC, a macroscopic number of eigenstates accumulate at one of the edges with a dominant directional hopping dependence, a manifestation of non-reciprocal hopping. We will discuss this aspect in more detail subsequently. Moreover, at the strong non-reciprocity limit (J_R or $J_L \rightarrow 0$), higher-order EPs appear with an algebraic multiplicity scaling with system size while the geometric multiplicity becomes unity. This indicates that all the bulk modes align to one state, which is exponentially localized at the edge under OBCs, leading to the violation of the celebrated bulk boundary correspondence. We will come back to these aspects later in this review.

B. Non-Hermitian Su-Schrieffer-Heeger Model

Next, we discuss another important non-Hermitian model, namely the non-Hermitian Su-Schrieffer-Heeger (SSH) model. It is a one-dimensional tight-binding model on a bipartite lattice with non-reciprocal intra-unit cell hopping and PT symmetric imaginary staggered potential [48–51]. We note that several other variants and generalizations also exist in the literature [52–59]. Notably, the parent Hermitian SSH model is paradigmatic in its own

right with several intriguing topological properties [60, 61]. The non-Hermitian SSH model Hamiltonian on a finite chain with L sites reads $H = H^{\text{hop}} + H^{\text{pot}}$, where

$$H^{\text{hop}} = - \sum_i [t_1(c_{i,A}^\dagger c_{i,B} + h.c.) + t_2(c_{i+1,A}^\dagger c_{i,B} + h.c.) + t_3(c_{i+1,B}^\dagger c_{i,A} + h.c.)] \\ + \sum_i \delta(c_{i,B}^\dagger c_{i,A} - c_{i,A}^\dagger c_{i,B}), \quad (15)$$

and

$$H^{\text{pot}} = i \sum_i \gamma(c_{i,A}^\dagger c_{i,A} - c_{i,B}^\dagger c_{i,B}). \quad (16)$$

Here $c_{i,\alpha}^\dagger (c_{i,\alpha})$ is the fermionic raising (lowering) operator at site i for sublattice $\alpha = A, B$ (see Fig. 3 (a)). Here t_1 and t_2 denote the intra- and inter-unit cell hopping amplitudes, respectively, and δ introduces a non-reciprocity only in the intra-unit cell hopping, thereby introducing non-Hermiticity in the system. Here t_3 represents the next-nearest neighbor hopping from sublattice A to B . We first consider $t_3 = 0$ for simplicity. The onsite imaginary potential with balanced gain-and-loss $\pm i\gamma$ incorporates PT symmetry in the model. We present a detailed discussion of different symmetry classes in different parameter regimes of the model in the next section.

Since the system possesses translational symmetry under PBC, the eigenvectors and eigenvalues can be parameterized by k . In k space, the Hamiltonian can be written as

$$H(k) = \begin{pmatrix} i\gamma & t_2 e^{-ik} + t_1 - \delta \\ t_2 e^{ik} + t_1 + \delta & -i\gamma \end{pmatrix}. \quad (17)$$

In the Hermitian limit, $\gamma = \delta = 0$. For both $t_1 < t_2$ and $t_1 > t_2$, the dispersion is gapped with a bond dimer-like order and different polarizations, which can be characterized by a Bloch topological invariant or winding number [61]. Here $t_1 = t_2$ is a gapless critical point separating these two gapped phases with different orbital characteristics. The topological phase with a nontrivial winding number gives rise to zero energy edge modes under OBC. Next, we consider two distinct cases of the non-Hermitian model parameters and discuss the topological features of both regimes.

(a) Symmetric intra-unit cell hopping ($\delta = 0$) in the presence of onsite potential ($\gamma \neq 0$): In this case, the model exhibits both PT symmetry broken and unbroken phases. Interestingly, the PT symmetry induces unique topological phase transition in the system. Unlike

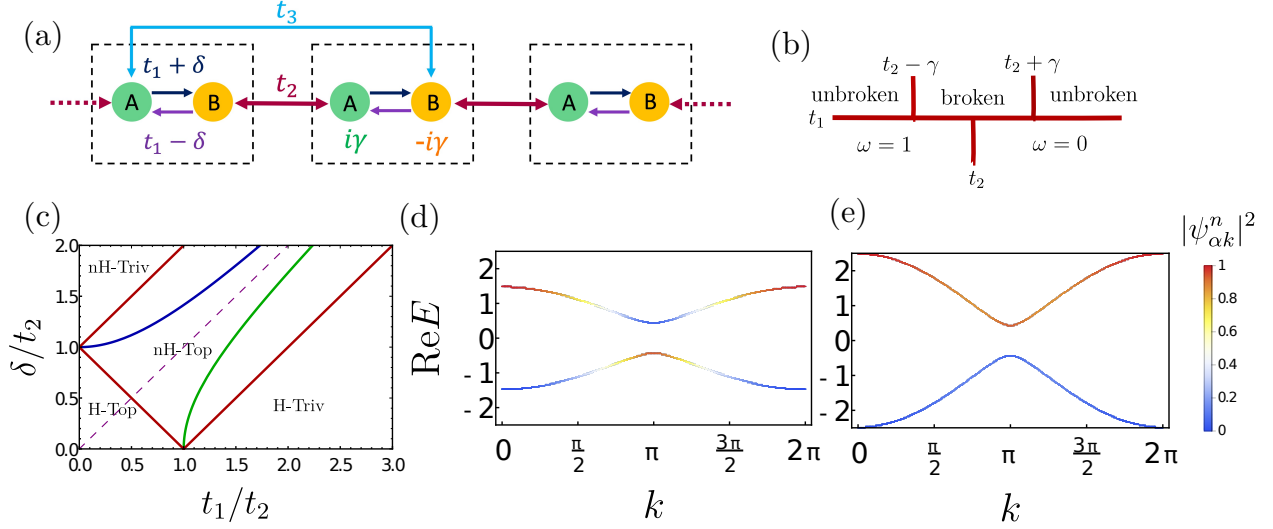


FIG. 3. **Non-Hermitian Su-Schrieffer-Heeger model.** (a) Schematic depiction of the generalized non-Hermitian Su-Schrieffer-Heeger model. Sublattice atoms A and B form the unit cell. The intra unit cell hopping is non-reciprocal, given by $t + \delta$ and $t_1 - \delta$ from left to right and right to left, respectively. The inter unit cell hopping strength is t_2 . Next-nearest neighbour hopping potential from sublattice A to B is given by t_3 . A non-Hermitian gain and loss has also been included on sublattices A and B , with strength γ . Here, δ and γ are the non-Hermitian parameters of the model. (b) The one-dimensional phase diagram with t_1 for the PT -symmetric case consists of PT broken and unbroken phases as a function of t_1 . Here ω is the topological index that counts the pairs of gapless-real-energy edge modes in the system. (c) Periodic (red) and open boundary condition (blue, green, and purple-dashed) phase diagram of the model in the absence of staggered potential ($\gamma = 0$) derived from the single-particle gap closings. (d) and (e) The distinction between H-top and H-triv phases through orbital band character. The real part of the dispersion is shown with $|\psi|^2$ contribution in color with $t_1 = 0.5$ and $\delta = 0.25$ (d), and $t_1 = 1.5$ and $\delta = 0.25$ (e). Note the difference in the orbital character around $k = \pi$ for the two cases. We choose $t_2 = 1.0$, $t_3 = 0$, and $\gamma = 0$.

the Hermitian SSH model, the edge modes can exist in the entire PT symmetry broken region as long as $t_1 < t_2$ even with bulk band crossing. The phase transition happens when bulk band merges with edge albeit with an imaginary gap in the dispersion. The topological phase transition is governed by a topological index, which a complex Berry phase can characterize [49]. We present the complete phase diagram in this phase in Fig. 3(b).

(b) Non-reciprocal hopping with non-zero δ in the absence of staggered potential ($\gamma = 0$): In this case, the Hamiltonian respects the sub-lattice symmetry $S : c_{iA} \rightarrow -c_{iA}^\dagger, c_{iB} \rightarrow c_{iB}^\dagger$, $SH^\dagger S^{-1} = H$, and $\sigma_z H(k) \sigma_z^{-1} = -H(k)$ [62]. Consequently, the energy eigenvalues come in \pm pairs at each k . We follow the notations introduced in Ref. [50] and discuss the detailed features of the system. The PBC phase diagram is divided into four regions considering the single-particle spectrum gap closings (for absolute values of energies) for lines $\delta = t_1 \pm 1$ and $\delta = 1 - t_1$ (see Fig. 3(c)): (i) Hermitian topological ($\delta < (1 - t_1)$) – the complex spectrum has a two-lobe structure with a real energy line gap in the complex plane $\{\text{Re}[E], \text{Im}[E]\}$. In subsequent Section V, we present a detailed discussion of various kinds of complex energy gaps. (ii) Hermitian trivial ($t_1 > 1 + \delta$) – spectral topology shows the structure similar to (i) (see Fig. 6(a)). Interestingly, both phases (i) and (ii) show distinctive features in terms of orbital band character, revealing their topological and trivial nature, respectively [63] (see Fig. 3 (d) and (e)). (iii) Non-Hermitian topological ($\delta > (|1 - t_1|), \delta < (1 + t_1)$) – the spectral topology changes to a single loop in the complex plane from a two-lobe structure in (i) via Lifshitz transitions (see Fig. 6 (b)). (iv) Non-Hermitian trivial ($\delta > (1 + t_1)$) – the complex spectrum comprises of two spectral lobes vertically displaced along the imaginary axis with an imaginary line gap. The phase transitions between different phases are marked by EPs with a significant change in spectral topology. The spectral topology of four regions [(i)-(iv)] are characterized by winding numbers (see Eq. 12) $(1, 1, 1/2, 0)$, respectively. Interestingly, similar to the Hatano-Nelson model, the existence of chiral modes and the finite winding numbers are interconnected and guaranteed by the symmetry-protected spectral topology [46, 64, 65]. For OBC, one finds four distinct regions as shown in Fig. 3 (c). Briefly, $\delta > t_1$ region leads to real eigenvalues, while for $\delta < t_1$, the eigenvalues are complex. Moreover, within the region $\sqrt{t_1^2 - 1} < \delta < \sqrt{t_1^2 + 1}$, one finds topological phases characterized by zero energy edge modes which are perturbatively connected to topological boundary modes in the Hermitian limit ($\delta = 0, t_1 < t_2$). The immediate incongruity between the PBC and OBC phase diagram stems from the non-Hermitian nature of the system, reflecting the extreme sensitivity to the boundary conditions. We will subsequently present various interesting features of the model, considering the intricate interplay of symmetry, spectral topology, and boundary sensitivity [50, 57, 66–77].

C. Non-Hermitian Chern Insulators

We now introduce a two-dimensional non-Hermitian Chern insulator model, which has been important in understanding higher dimensional non-Hermitian phases. We will explain its topological characterization in terms of the non-Hermitian generalization of the Chern number following pioneering work in Refs. [29, 78]. The momentum space Hamiltonian of the system reads

$$H(\mathbf{k}) = (v_x \sin k_x + i\gamma_x)\sigma_x + (v_y \sin k_y + i\gamma_y)\sigma_y + (m - t_x \cos k_x - t_y \cos k_y + i\gamma_z)\sigma_z. \quad (18)$$

The Hermitian part of the model corresponds to the Qi-Wu-Zhang model [79], whereas the non-Hermitian parameters γ_i ($i = x, y, z$) describe the imaginary coupling between the orbitals, which can be thought as a manifestation of imaginary Zeeman field [80]. In the Hermitian limit, $\gamma_{x,y,z} = 0$, the model exhibits topological phase transitions at $m = t_x + t_y$, where the Chern number switches.

Before we go to the topological characterization of this Chern insulator model, we take a brief detour and discuss the topological band theory for a non-Hermitian Hamiltonian with the generalized notion of gapped band structures in the complex parameter plane introduced by Shen *et al.* [80]. For a non-Hermitian Hamiltonian of a periodic system, the Bloch theorem suggests that the energy eigenvalues can be parameterized by crystal momentum \mathbf{k} in the Brillouin zone, thus defining a band structure. A band labelled by index n is called "gapped" or "separable" if its energies in the complex plane do not overlap with that of any band. More precisely, one can define a band to be separable if its energy $E_n(\mathbf{k}) \neq E_m(\mathbf{k})$ for all $m \neq n$ and all \mathbf{k} . In contrast, a band is called inseparable if at some momentum \mathbf{k} the complex energy $E_n(\mathbf{k})$ overlaps with another band $E_m(\mathbf{k})$ and becomes degenerate. We can now define the non-Hermitian version of the Chern number defined over the Brillouin zone for an energy band in two dimensions, which serves as the basis of topological classification in non-Hermitian systems. For a separable band structure ($\langle \psi_n^L | \psi_n^R \rangle \neq 0$), with energy E_n , the Chern number can be defined as [29]

$$C_n^{\Theta\nu} = \frac{1}{2\pi} \int_{\text{BZ}} \epsilon_{ij} B_{n,ij}^{\Theta\nu}(\mathbf{k}) d^2\mathbf{k}, \quad (19)$$

where $\epsilon_{ij} = -\epsilon_{ji}$ and $B_{n,ij}^{\Theta\nu}(\mathbf{k}) = i\langle \partial_i \psi_n^{\Theta}(\mathbf{k}) | \partial_j \psi_n^{\nu}(\mathbf{k}) \rangle$, with the normalization condition

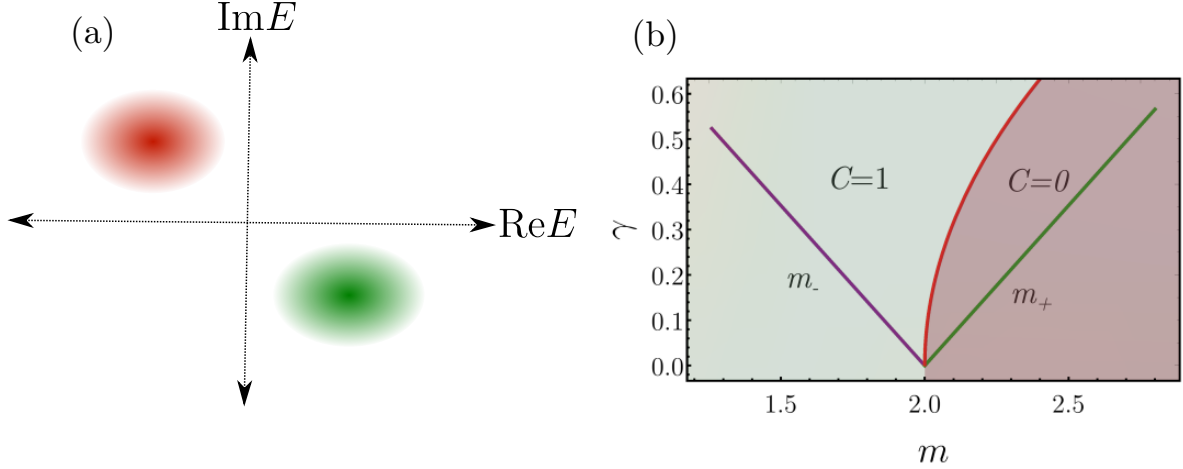


FIG. 4. **Non-Hermitian Chern insulator.** (a) The notion of separable bands. The energies of the two bulk bands are shown in red and green regions. (b) Topological phase diagram based on open boundary spectra, Bloch, and non-Bloch Chern numbers. The Bloch-Hamiltonian phase boundaries are shown as the green and solid purple lines denoted by straight lines $m = m_{\pm}$. The non-Bloch Chern number C , defined in Eq. 23, predicts the presence of non-trivial chiral edge states in the blue-shaded area with the non-Bloch Chern number $C = 1$. The phase boundary dividing the topological and trivial regions can be well approximated by the red line denoted by the curve $m = 2 + \gamma^2$.

$\langle \psi_n^{\Theta}(\mathbf{k}) | \psi_n^{\nu}(\mathbf{k}) \rangle = 1$. Here $\Theta, \nu = L/R$, where L/R represent the left and right eigenvectors. Interestingly, Ref. [29] shows that all four combinations of Chern numbers are equal $C^{LL} = C^{LR} = C^{RL} = C^{RR}$, characterizing the same topological features of a band.

Coming back to the non-Hermitian Chern insulator model, we find that the Bloch spectrum is gapped for $m > m_+$ and $m < m_-$ and the Chern number becomes 0 and 1 respectively. Here $m_{\pm} = t_x + t_y \pm \sqrt{\gamma_x^2 + \gamma_y^2}$ with $\gamma_z = 0$. The gap closes at the Bloch phase boundaries for $m = m_{\pm}$ and the Chern number is undefined in between these phase boundaries (see Fig. 4 (b)). Strikingly, the Bloch Chern number dramatically fails to mimic the edge state information of the corresponding open boundary system. The dissimilarity between open boundary and periodic boundary Bloch spectra results in the violation of conventional bulk-boundary correspondence [41]. The resolution to this puzzle comes from the non-Bloch band theory proposed by Yao *et al.* [78], which will be discussed in detail in Section VII. Briefly, the non-orthogonal nature of eigenvectors suggests an exponential

profile of bulk eigenstates, which in turn demands a modification in the Bloch wavevector with an imaginary component. The formalism goes as follows. The low energy continuum model for the Chern insulator up to order k_j^2 can be written as

$$H(\mathbf{k}) = (v_x k_x + i\gamma_x)\sigma_x + (v_y k_y + i\gamma_y)\sigma_y + (m - t_x - t_y + \frac{t_x}{2}k_x^2 + \frac{t_y}{2}k_y^2)\sigma_z, \quad (20)$$

$$= H_0 + H_1,$$

where $H_1 = i\gamma_x\sigma_x + i\gamma_y\sigma_y$ and H_0 is the remaining part of the Hamiltonian. For small \mathbf{k} , H_1 can be thought as the first-order response of H_0 , i.e., $H_1 = i\sum_{j=x,y} \frac{\gamma_j}{v_j} \frac{\partial H_0}{\partial k_j} = \sum_j \frac{\gamma_j}{v_j} [x_j, H_0]$. This problem can be solved considering H_1 as a perturbation. The lowest order perturbation to an eigenfunction of H_0 takes the form $\exp[(\gamma_x/v_x)x + (\gamma_y/v_y)y]$. This suggests that we need a complex-valued wavevector to describe the open boundary eigenstate

$$\mathbf{k} \rightarrow \tilde{\mathbf{k}} + i\tilde{\mathbf{k}}', \quad (21)$$

where $\tilde{k}_j = -\gamma_j/v_j$ for small $\tilde{\mathbf{k}}'$ in this model. One can write the non-Bloch Hamiltonian as

$$\tilde{H}(\tilde{\mathbf{k}}) = H(\mathbf{k} \rightarrow \tilde{\mathbf{k}} + i\tilde{\mathbf{k}}'). \quad (22)$$

Now one can define the non-Bloch Chern number in terms of left and right eigenvectors parameterized by $\tilde{\mathbf{k}}$

$$C_n^{\tilde{\Theta}\nu} = \frac{1}{2\pi} \int_{\tilde{T}^2} \epsilon_{ij} B_{n,ij}^{\tilde{\Theta}\nu}(\tilde{\mathbf{k}}) d^2\tilde{\mathbf{k}}, \quad (23)$$

over the generalized Brillouin zone $\tilde{T}^2(\tilde{\mathbf{k}})$. The non-Bloch Chern number can precisely predict the topological boundary states under OBC with topological phase boundary at $m = 2 + \gamma^2$ separating the two distinct phases with non-Bloch Chern numbers 0 and 1 (see Fig. 4 (b)).

D. Non-Hermitian Topological Semimetals

In recent years the concepts of topology have been extended to gapless systems, such as nodal semimetals [8, 81–85]. They host topologically protected stable degeneracies, which

lead to intriguing properties owing to their distinctive electronic excitations. The effect of non-Hermiticity in such systems has been an emerging area of research in the last years. The presence of EPs in the dispersion fundamentally changes the nature of nodal semimetals resulting in various kinds of exceptional manifolds, such as lines, rings, surfaces, and complex nexus structures in different dimensions [86–96]. Remarkably, the generalized notion of the energy gap in a complex plane introduces multiple topological structures with distinct gapless phases truly unique to non-Hermitian systems [62, 97–100]. For instance, due to topological protection of EPs, one can obtain an open Fermi arc around an EP with fractional topological charge in direct contrast to conventional Dirac and Weyl semimetals [101, 102]. Interestingly, the ramified symmetry classification in non-Hermitian systems enriches the catalog of symmetry protected topological phases [64, 103–105]. Recent studies show that various non-Hermitian spatial symmetries, which act non-locally in the momentum space, can stabilize an exceptional unconventional Weyl semimetal by enforcing general constraints on band degeneracies [106]. Ref. [103] has put forward important examples of symmetry protected topological phases governed by generic non-Hermitian symmetries, which act on the Hamiltonian in the following way $H = QH^\dagger Q^{-1}$, $Q^\dagger Q^{-1} = QQ^\dagger = \mathbb{I}$.

As we discussed previously, Eq. 5 and Eq. 6 suggest that tuning two parameters can lead to non-Hermitian phases with a substantial reduction in spatial dimension compared to their Hermitian counterpart. As an illustration, let us consider Eq. 5, which respects $H = QH^\dagger Q^{-1}$ with $Q = \sigma_x$. It trivially satisfies the condition $\mathbf{f}_R \cdot \mathbf{f}_I = 0$, allowing a one parameter tuning to obtain an exceptional structure. Consequently, one obtains EPs, exceptional lines, and surfaces in one, two, and three-dimensional systems, respectively. The eigenvalues of the system read $\epsilon_\pm = \pm\sqrt{f_R^2 - f_I^2}$ which suggests either purely real (or imaginary) eigen structures with non-Hermitian Fermi arcs manifesting the branch cut singularities connecting the EPs with a crucial distinction in dispersion [107] (see Fig. 5). Consequently, non-Hermitian Fermi arcs, which are a bulk phenomenon, fundamentally differ from surface Fermi arcs in conventional Weyl semimetals [8]. Interestingly, the two-dimensional Weyl node in the Hermitian phase with semi-metallic band structure turns into a metallic dispersion in the presence of EPs due to parameter redundancy [102]. Very recently, topological semimetals have attracted much interest in terms of broken and unbroken bulk boundary correspondence under OBC [67, 68, 108–110]. Among them, the topological features of non-Hermitian nodal semimetals [111], semi-Dirac semimetals [112],

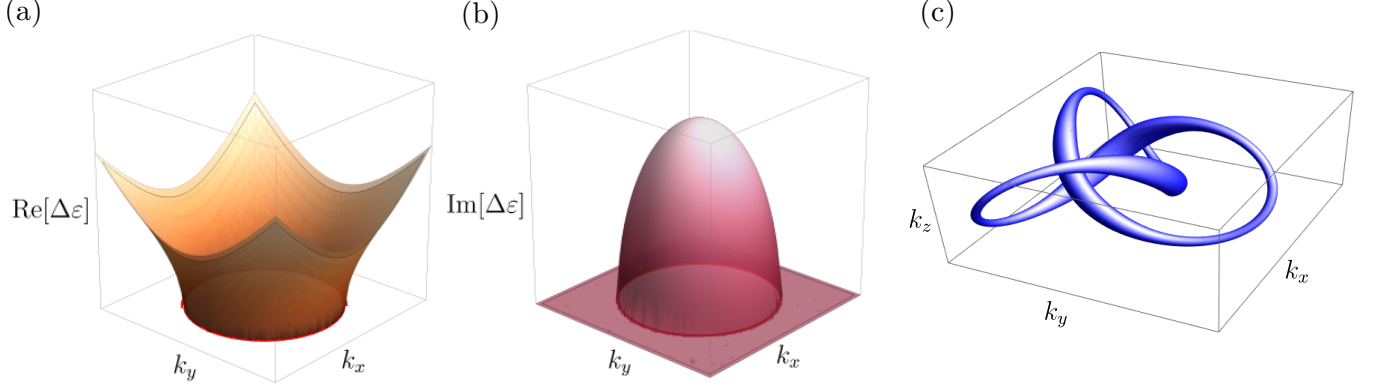


FIG. 5. **Non-Hermitian topological metals.** (a) The real (orange) and (b) imaginary (magenta) parts of the spectral gap ε as a function of momentum in a two-dimensional Weyl node in the presence of onsite gain and loss, illustrating a generic symmetry-protected non-Hermitian nodal phase. Contours of exceptional points are indicated by red lines, separating two disparate regions where the real energy is projected to zero (open Fermi volumes) from those where the imaginary part of ε vanishes. The exceptional ring is symmetry protected with $\sigma_x H^* \sigma_x = H$, which constrains this particular kind of eigen structure of both components. (c) Illustration of an exceptional nodal knotted semimetals for the Hamiltonian of the form $H(\mathbf{k}) = f_1(\mathbf{k})\sigma_x + f_3(\mathbf{k})\sigma_z$.

and Weyl semimetals [113] are worth mentioning.

Topological nodal line semimetals can display symmetry-protected knotted line degeneracies in momentum space in Hermitian systems [114–122]. Remarkably, non-Hermitian topological phases in three dimensions can give rise to knotted phases with robust band degeneracies even in the *absence* of any symmetry [123, 124]. For instance, one can transit from nodal line semimetals to twisted Hopf link exceptional lines via Lifshitz transitions with distinctive changes in the Fermi surface characterized by a topological linking number without any symmetry constraint [123]. The knotted phase with metallic dispersion can be characterized by open Fermi surfaces with vanishing real energy gaps, known as Seifert surfaces, that are bounded by knotted lines of EPs [125, 126]. The eigenenergy strings of the knotted structures can provide complete information on topological classifications and concomitant phase transitions of non-Hermitian Hamiltonians with separable bands in terms of their respective knot invariants and braiding patterns [127]. Interestingly, non-Hermitian nodal knot metals with delicate complex energy eigenbands lead to unique surface states, dubbed as *tidal* surface states, which are related to band vorticity and layer structure of

their dual Seifert surface, revealing the algebraic, geometric, and topological aspects of their parent knots [128].

Tuning of various topological semimetallic band structures has become an active topic of current research owing to their interesting geometry and fascinating transport properties both in Hermitian [129–138] and non-Hermitian systems [139–146]. Hermitian Hamiltonians hosting Weyl points with arbitrary topological charge can be transformed to one-dimensional exceptional contours in the presence of non-Hermitian gain-and-loss perturbations [30, 146]. Tuning of such non-Hermitian perturbations leads to a new class of topological phase transitions via merging of oppositely charged exceptional contours [30]. For example, in Ref. [147], the authors discuss the disorder-driven topological phase transitions in type-II Weyl semimetals, where type II Weyl points transform into a flat band or a nodal line segment depending on the tilt direction. Recent studies show that symmetry-protected two-dimensional non-Hermitian topological phases can be realized by tuning the staggered asymmetric hopping strengths in a one-dimensional superlattices [148]. On the other hand, Floquet engineering – tuning properties of quantum systems using periodic driving – is a useful tool to manipulate quantum matter [149, 150]. It has been recently shown that periodic driving may be used to control the positions and stability of EPs in non-Hermitian topological semimetals [151]. One can simulate non-Hermitian semimetals exhibiting exceptional rings through driving, and associated topological phase transitions arising from the application of light can be traced out by nontrivial Hall conductivity [152]. Furthermore, recent studies show that driving can be used as a facile tool to generate exceptional contours. The charge division of the created exceptional contours and the concomitant Lifshitz transitions have been studied in non-Hermitian multi-Weyl semimetals in the presence of circularly polarized light [153]. One can also tailor and control other higher-order topological phases exhibiting two-dimensional corner and three-dimensional hinge states by tuning the gain and loss or periodic driving [154–156]. Floquet engineering of non-Hermitian topological matter thus seems to be a promising future avenue [141, 143, 144, 157].

IV. NON-HERMITIAN SYMMETRY CLASSES

The well-known Altland-Zirnbauer classification of Hermitian topological insulators and superconductors [158], which segregates Hermitian systems into 10 distinct symmetry classes

based on the presence or absence of three internal symmetries – time-reversal symmetry (TRS), particle-hole symmetry (PHS) and chiral symmetry (CS) – is modified in the presence of non-Hermiticity [46, 69, 104, 159–163]. Non-Hermiticity results in the ramification and, in some cases, a unification of these symmetry classes, as shown by Kawabata *et al.* [64]. The fundamental difference which leads to recasting the symmetry classification is that for non-Hermitian systems $H^\dagger \neq H$ and hence, $H^T \neq H^*$. This leads to the bifurcation of PHS and CS under non-Hermiticity. To illustrate, a Hermitian system with PHS follows $CH^*C^{-1} = -H$, where C is a unitary operator. Since complex conjugation and transposition are not equivalent operations for non-Hermitian systems, PHS gets ramified as $CH^*C^{-1} = -H$ and $CH^TC^{-1} = -H$. Similarly, for Hermitian systems CS follows $\Gamma H \Gamma^{-1} = -H$; under non-Hermiticity, this separates into $\Gamma H \Gamma^{-1} = -H$ and $\Gamma H^\dagger \Gamma^{-1} = -H$ where Γ is a unitary operator. Moreover, TRS being an antiunitary symmetry follows either of the following in Hermitian systems, $T_+ H^* T_+^{-1} = H$ or $T_- H^* T_-^{-1} = -H$. However, a non-Hermitian Hamiltonian H can be directly mapped to iH with a one-to-one correspondence. Hence, $T_+ H^* T_+^{-1} = H$ implies $T_+ (iH)^* T_+^{-1} = -(iH)$, making $T_+ \equiv T_-$, unifying both symmetries. @articleashida2020non, @articleashida2020non, These internal symmetries of a non-Hermitian system (C , T and Γ such that $CC^* = \pm 1$, $TT^* = \pm 1$, and $\Gamma^2 = 1$), along with pseudo anti-Hermiticity (PAH) – $\eta H^\dagger(k) = \eta^{-1} = -H(k)$ where $\eta^2 = 1$ – form the generators of the non-Hermitian symmetry classification [49, 103, 161, 164, 165]. The interplay of non-Hermiticity and these discrete symmetries leads to a 38-fold symmetry classification summarized in Table I. Further, more recent studies show that time-independent non-Hermitian systems with a line gap, as well as time-dependent Floquet non-Hermitian systems can be classified into 54 different non-Hermitian symmetry classes, as shown in Refs. [19, 163, 166].

One of the interesting consequences of this modification of symmetry classes is that despite topological phases being impossible in the one-dimensional class AI for Hermitian systems, the presence of non-Hermiticity leads to a possibility of topologically protected edge states. Remarkably, these zero-mode energy states in the non-Hermitian one-dimensional symmetry class AI have been experimentally observed in photonic lattices [167]. The classification of non-Hermitian symmetries also leads to the systematic prediction of symmetry-protected topological lasers, as shown in Ref. [64], which can have several physical applications.

TABLE I. **Classification of non-Hermitian symmetries.** Combinations of each group of symmetries (i.e. each column) give rise to 10 symmetry classes giving a total of $4 \times 10 = 40$ symmetry classes. However, there are some redundancies in counting. For example, the symmetry-less class A has been counted 4 times – once in each group. The correct combinations accounting for redundancies gives rise to the 38-fold classification of non-Hermitian symmetries. Here, TRS_c and TRS_t denote the symmetry considering conjugation and transposition of H respectively. Similarly, for PHS_c and PHS_t .

$\text{TRS}_c : H = TH^*T^\dagger$	$\text{TRS}_t : H = TH^TT^\dagger$	$\text{TRS}_c : H = TH^*T^\dagger$	$\text{TRS}_t : H = TH^TT^\dagger$
$\text{PHS}_c : H = -CH^*C^\dagger$	$\text{PHS}_t : H = -CH^TC^\dagger$	$\text{PHS}_t : H = -CH^TC^\dagger$	$\text{PHS}_c : H = -CH^*C^\dagger$
$\text{CS} : H = -\Gamma H \Gamma^{-1}$	$\text{CS} : H = -\Gamma H \Gamma^{-1}$	$\text{PAH} : H = -\eta H^\dagger \eta^{-1}$	$\text{PAH} : H = -\eta H^\dagger \eta^{-1}$

As a concrete illustration, we present the symmetries in the generalized non-Hermitian SSH model described previously in Fig. 3(a). We tabulate each symmetry along with their constraint equations and symmetry operators in Table II and highlight the conditions under which it is possible to obtain the specific symmetry. By imposing certain constraints on the system parameters, it is possible to transition between different symmetry conditions.

V. COMPLEX ENERGY GAPS IN NON-HERMITIAN SYSTEMS

Unlike in Hermitian systems, the complex energy eigenvalues of non-Hermitian Hamiltonians cannot be ordered from lowest to highest, making the task of defining an energy gap non-trivial. Two kinds of complex energy gaps have been postulated to exist in non-Hermitian spectra [64] – point gap and line gap (illustrated in Fig. 6 for the non-Hermitian SSH model). A point gap can be defined as a point in the complex plane where no energy eigenstates exist. Unitary flattening of the spectrum cannot lead to crossing that particular point. Any non-Hermitian Hamiltonian with a point gap can be deformed to a unitary matrix which preserves the point gap and its symmetries. On the other hand, a line gap is defined as an infinite line in the complex plane with no eigenenergy crossings. A line gap can, in general, be arbitrary. However, in the presence of TRS, the real axis forms the line gap, while under CS, the line gap becomes the imaginary axis. A non-Hermitian Hamiltonian with a line gap can be flattened to a Hermitian matrix which preserves the line gap

TABLE II. **Symmetry conditions for generalized non-Hermitian Su-Schrieffer-Heeger model.** Each symmetry has its own constraint equation which is satisfied by the symmetry operator acting on the Hamiltonian. The conditions on the system parameters required to preserve the symmetry is given in the last column. The symbol ‘ \times ’ denotes that under no condition can the non-Hermitian SSH model preserve the corresponding symmetry.

Symmetry	Equation	Operator	Conditions
PHS _t , $CC^* = 1$	$H(-k) = CH^T(k)C^\dagger$	\mathbb{I}_2	$t_2 = t_3, \delta = 0$
PHS _t , $CC^* = -1$	$H(-k) = CH^T(k)C^\dagger$	$i\sigma_y$	\times
TRS _t , $TT^* = 1$	$H(-k) = TH^T(k)T^\dagger$	\mathbb{I}_2	$t_2 = t_3, \delta = 0$
TRS _t , $TT^* = -1$	$H(-k) = CH^T(k)C^\dagger$	$i\sigma_y$	\times
PHS _c , $CC^* = 1$	$H(-k) = -CH^*(k)C^\dagger$	\mathbb{I}_2	\times
PHS _c , $CC^* = -1$	$H(-k) = -CH^*(k)C^\dagger$	$i\sigma_y$	$t_2 = t_3, \delta = 0, \gamma = 0$
TRS _c , $TT^* = 1$	$H(-k) = TH^*(k)T^\dagger$	\mathbb{I}_2	$t_2 = t_3, \gamma = 0$
TRS _c , $TT^* = -1$	$H(-k) = TH^*(k)T^\dagger$	$i\sigma_y$	\times
CS	$H(k) = -\Gamma H^\dagger(k)\Gamma^{-1}$	σ_z	$t_2 = t_3, \delta = 0$
PAH	$H(k) = -\eta H^\dagger(k)\eta^{-1}$	σ_x	\times
Pseudo-Hermiticity	$H(k) = \zeta H^\dagger(k)\zeta^{-1}$	σ_x	$t_2 = t_3$
Sublattice symmetry	$H(k) = -SH(k)S^{-1}$	σ_z	$\gamma = 0$
Parity	$H(-k) = PH(k)P^{-1}$	σ_x	$t_2 = t_3, \delta = 0, \gamma = 0$
Parity-time	$H(k) = (PT)H^*(k)(PT)^{-1}$	σ_x	$t_2 = t_3, \delta = 0$
Parity-Particle hole	$H(k) = -(CP)H^*(k)(CP)^{-1}$	σ_x	\times
Inversion	$H^\dagger(-k) = IH(k)I^{-1}$	σ_z	\times

and its symmetries. Hence, systems with a point-gap topology are inherently non-Hermitian with no correspondence to a Hermitian Hamiltonian. As such the presence of a point gap topology leads to intrinsically non-Hermitian phenomena [65, 69, 74, 168, 169]. We next discuss one such non-Hermitian phenomenon, namely the non-Hermitian skin effect.

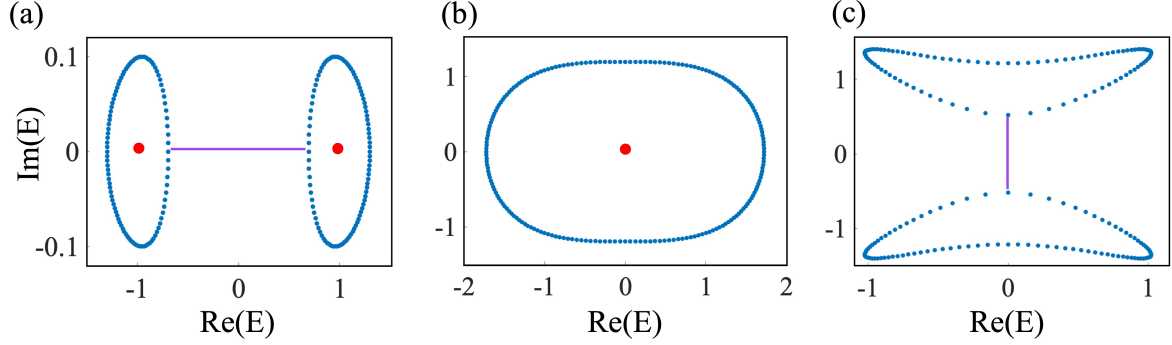


FIG. 6. **Point gaps and line gaps in the different phases in the non-Hermitian Su-Schrieffer-Heeger model.** (a) Prototype of the complex energy spectrum in the Hermitian phases (Hermitian topological or trivial phase) showing point gaps within the two spectral loops (shown by the red dots) and a real line gap separating energy loops (shown by the purple line). (b) The non-Hermitian topological phase has a point gap at zero energy shown by the red dot. (c) The non-Hermitian trivial phase which has an imaginary line gap between the two complex spectral loops (shown in purple).

VI. NON-HERMITIAN SKIN EFFECT

The non-Hermitian skin effect (NHSE) is a phenomenon completely unique to non-Hermitian systems, where a maximal number of eigenstates localize at the system's edges under OBC [21, 170–175]. The NHSE has been theorised in several non-Hermitian systems in one [170, 173], two [176–178] and three dimensions [172, 179]. We note that the effect has also been recently observed experimentally in photonic systems [168, 177, 180–182], acoustic topological insulators [183, 184], and topoelectrical circuits [185–189], to highlight a few.

In order to intuitively understand the NHSE, we can consider the minimal non-Hermitian SSH model with non-reciprocal hopping, as shown in Fig. 3(a). We can ignore the on-site energies and the next nearest neighbour hopping t_3 for this discussion. The directionally-favoured hopping leads to a persistent current in the system under PBC, which results in the accumulation of the eigenstates at a boundary when OBC is imposed. This interrelation of the current in PBC and the NHSE in OBC was recently enunciated by Zhang *et al.* [190]. The unit cell current under PBC can be calculated according to Ref. [61] as

$$J = \frac{iL}{2} [\langle c_j^\dagger c_{j+1} \rangle - \langle c_{j+1}^\dagger c_j \rangle], \quad (24)$$

where L is the length of the SSH chain, c_j^\dagger and c_j are the fermionic creation and annihilation operators at site j , respectively. Here j denotes any lattice site in the chain since the same current flows throughout the system. For a one-dimensional system, the presence of a persistent current directly relates to a non-zero winding of eigenenergies in the complex plane as demonstrated in Ref. [190], establishing that the non-zero winding number under PBC implies an NHSE under OBC and vice-versa. Further, the presence of either indicates a persistent current under PBC. The relationship between the skin effect with the winding number suggests that the NHSE originates due to the inherent topology of non-Hermitian systems, established by Okuma *et al.* [191]. The necessary and sufficient conditions to obtain a skin effect under OBC can be summarised as follows: (a) in one-dimensional systems, the PBC complex energy spectrum must exhibit a point-gap topology [191], and (b) in two or higher dimensions, the eigenspectrum under PBC must accommodate a finite spectral area in the complex plane [192].

Internal symmetries of the underlying non-Hermitian Hamiltonian can also play an interesting role in determining the nature of NHSE that the system demonstrates. For example, in systems preserving TRS, such as quantum spin Hall insulators, where the \mathbb{Z}_2 invariant becomes non-trivial, the eigenstates form Kramers pairs, one of which localizes at the left boundary while the other localizes at the right boundary under OBC. This type of symmetry-protected NHSE has been dubbed the \mathbb{Z}_2 skin effect [191]. The interplay of non-Hermiticity and symmetries can also give rise to higher-order NHSE, where skin modes are localized at the corners of a sample rather than the edges. This has been exhibited in Refs. [155, 172, 183, 193]. Furthermore, Lu *et al.* [194] study the interplay of magnetic field and NHSE. Interestingly, they discover that magnetic fields can strongly suppress the NHSE despite its topological origin.

VII. BROKEN BULK-BOUNDARY CORRESPONDENCE AND THE GENERALIZED BRILLOUIN ZONE

In general, for topological phases of Hermitian systems, there exists a topological invariant which depends on the bulk properties of the system, which can predict the number of

zero energy boundary states the system will exhibit [6]. The existence of edge states solely depends on the bulk of the system. This makes them robust to perturbations and hence topological in nature. However, the presence of non-Hermiticity, leads to a failure of the conventional bulk boundary correspondence [41, 43, 67, 181, 186, 195]. The NHSE, which is accompanied by the drastic localization of all eigenstates, demonstrates the strikingly different behaviour of the system at the bulk and the boundary. This extreme sensitivity of non-Hermitian systems to their boundary conditions leads to the broken bulk boundary correspondence, which posed a considerable challenge. For instance, winding numbers calculated for the bulk cannot predict the number of boundary states as there is a significant difference between the PBC and the OBC spectra.

In order to resolve this problem and establish a generalized bulk boundary correspondence, the notion of a generalized Brillouin zone (GBZ) was proposed by Yao and Wang [51]. Here, the usual Bloch phase factor e^{ik} is replaced by a non-Bloch phase factor $\beta = re^{ik}$ for the system under PBC, where the system parameters determine r . This implies that the wavevector acquires an extra imaginary factor such that $k \rightarrow k - i \ln r$. Here β can take values in a non-unit circle $|\beta| = r$, which defines the GBZ. The non-Bloch Hamiltonian, $H(\beta)$, can now be used to calculate a winding number W_{GBZ} over the GBZ, and $2W_{\text{GBZ}}$ determines the number of robust zero energy modes at the boundaries of the system under OBC. This generalized Bloch band theory helps substantiate the generalized bulk boundary correspondence for non-Hermitian systems, which was further demonstrated by Yokomizo and Murakami in one-dimensional systems [196]. Moreover, to explain the occurrence of the NHSE under OBC, a similar effective Hamiltonian $H(\beta)$ can be written in terms of the GBZ, where β is determined by the system parameters. To illustrate, for a one-dimensional tight-binding model on a bipartite lattice, according to Ref. [111], the eigenstates on lattice sites A and B can be written as $(\psi_{An}, \psi_{Bn}) = \beta^n(\psi_A, \psi_B)$, where n denotes the n -th lattice site. When $\beta = 1$, all the eigenstates are extended. However, $\beta \neq 1$ implies an NHSE, where $\beta < 1$ and $\beta > 1$ signify localization of the states at opposite edges, establishing a connection between the boundary-behaviour and the bulk Hamiltonian under OBC.

As a concrete example, let us consider the generalized non-Hermitian SSH model (as shown in Fig. 3(a)) and construct the GBZ closely following the methods specified in Refs. [51, 196]. The real space Schrödinger equations for the SSH model can be written as

$$\begin{aligned}
t_2\psi_{B_{n-1}} + t_3\psi_{B_{n+1}} + (t_1 + \delta)\psi_{B_n} + i\gamma\psi_{A_n} &= E\psi_{A_n}, \\
t_2\psi_{A_{n+1}} + t_3\psi_{A_{n-1}} + (t_1 - \delta)\psi_{A_n} - i\gamma\psi_{B_n} &= E\psi_{B_n}.
\end{aligned} \tag{25}$$

Now, we consider the ansatz $(\psi_{A_n}, \psi_{B_n}) = \beta^n(\psi_A, \psi_B)$. Then, the above equations become

$$\begin{aligned}
t_2\beta^{-1}\psi_B + t_3\beta\psi_B + (t_1 + \delta)\psi_B + i\gamma\psi_A &= E\psi_A, \\
t_2\beta\psi_A + t_3\beta^{-1}\psi_A + (t_1 - \delta)\psi_A - i\gamma\psi_B &= E\psi_B.
\end{aligned} \tag{26}$$

Multiplying the equations and cancelling $\psi_A\psi_B$ from both sides gives us

$$(t_2\beta^{-1} + t_3\beta + t_1 + \delta)(t_2\beta + t_3\beta^{-1} + t_1 - \delta) = E^2 + \gamma^2. \tag{27}$$

From this, we obtain a quadratic equation in β as follows

$$\begin{aligned}
t_2t_3\beta^4 + (t_1t_3 + t_1t_2 - \delta(t_3 - t_2))\beta^3 + (t_2^2 + t_3^2 + t_1^2 - \delta^2 \\
-\gamma^2 + E^2)\beta^2 + (t_1t_2 + t_1t_3 + \delta(t_3 - t_2))\beta + t_2t_3 = 0.
\end{aligned} \tag{28}$$

In order to obtain the trajectory of the GBZ (C_β), β must satisfy the condition $|\beta_i| = |\beta_j|$ for a pair $i \neq j$. The above equation is of the form $f(\beta) = -E^2$. We consider $\beta' = \beta e^{ik}$ such that $k \in \mathbb{R}$, which will also satisfy $f(\beta') = -E^2$. Taking the difference of $f(\beta) - f(\beta')$, we arrive at a quadratic equation for $\beta(k)$ of the form

$$\begin{aligned}
t_2t_3\beta^2(1 - e^{2ik}) + (t_1t_3 + t_1t_2 - \delta(t_3 - t_2))\beta(1 - e^{ik}) + (t_1t_2 \\
+ t_1t_3 + \delta(t_3 - t_2))\beta^{-1}(1 - e^{-ik}) + t_2t_3\beta^{-2}(1 - e^{-2ik}) = 0,
\end{aligned} \tag{29}$$

Plotting $\beta(k)$ in the complex plane for $k \in [0, 2\pi]$, we obtain the trajectory C_β shown in Fig. 7(a). When the non-Hermiticity $\delta = 0$, C_β becomes a unit circle ($|\beta| = 1$) shown by the black dashed lines. The blue and red curves show C_β for different values of t_3 and δ . The GBZ corresponding to the blue curves is shown in Fig. 7(b) where β_2 and β_3 have been plotted such that the condition $|\beta_1| \leq |\beta_2| = |\beta_3| \leq |\beta_4|$ is satisfied. $|\beta| \neq 1$ implies the existence of NHSE in the system under OBC.

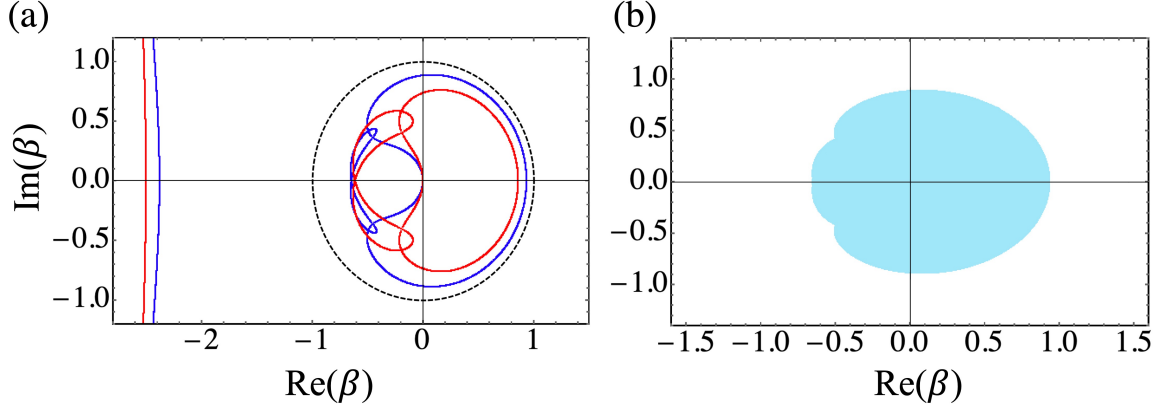


FIG. 7. **The generalized Brillouin zone for the non-Hermitian SSH model.** (a) The black dashed lines correspond to the Hermitian case of the SSH model where the GBZ is a unit circle. The blue curves show C_β where $t_3 = 1/3$ and the non-reciprocal hopping $\delta = 1/4$. The red curves correspond to $t_3 = 2/5$ and $\delta = 2/3$. C_β in the presence of t_3 and non-Hermiticity distorts from a circle. The C_β trajectories have been plotted such that $|\beta_i| = |\beta_j|$ ($i \neq j$). (b) The GBZ for the case corresponding to the blue curves ($t_3 = 1/3, \delta = 1/4$). Here, we plot the trajectories of β_2 and β_3 , such that, $|\beta_1| \leq |\beta_2| = |\beta_3| \leq |\beta_4|$. For all plots the values of other parameters are chosen to be $t_1 = 1.3$, $t_2 = 1.5$ and $\gamma = 0.5$.

VIII. DISORDER EFFECTS IN NON-HERMITIAN SYSTEMS

Disorder, being ubiquitous in nature, has gained a lot of interest [161, 178, 197–199], including in the context of non-Hermitian settings. The interplay of disorder and non-Hermiticity has led to the discovery of several new physical phenomena, some entirely unique to non-Hermitian systems [157, 199–203]. The study of disorder leads to the requirement of quantities which are ‘self-averaging’ under disorder, i.e., good indicators which should be independent of the exact disorder configuration but should depend only on the strength and the nature of the disorder introduced. Mondragon-Shem *et al.* [204] introduced a real-space winding number which is self-averaging, robust and remains quantized even at strong disorder values. Though this was proposed for Hermitian systems, this formalism was later extended to disordered non-Hermitian cases as well. A change in the winding number at a critical disorder strength leads to a phase transition where they have analytically proven that the localization length diverges. Localization transitions induced by non-Hermitian

disorder was further elucidated in one- [205, 206], two- [207, 208], and three-dimensional systems [209–211], as well as in non-Hermitian quasi-periodic crystals [212, 213]. Another exciting report by Hamazaki *et al.* [214] showed that in a time-reversal symmetric non-Hermitian system disorder-induced many-body localization can lead to a complex to real transition of the energy eigenspectrum. Refs. [159, 210] explored the behaviour of critical exponents and report on how non-Hermiticity modifies the universality classes of Anderson transitions. Another interesting recent discovery is the ‘non-Hermitian topological Anderson insulator’ – a normal insulator which transforms into a topological insulator under the effect of disorder and is characterized by a change in the topological winding number and occurrence of zero energy edge modes [157, 215–217]. Further, in Ref. [147], the authors showed that disorder in a type-II non-Hermitian Weyl semimetal can exhibit a flat band. Longhi [199] studied the role of different kinds of disorder in the Hatano-Nelson model by investigating the deformations in the radius of the complex energy spectrum. He discovered three disorder-induced phases in the model under both PBC and OBC, which was further confirmed by Sarkar *et al.* for the non-Hermitian SSH model [218]. Claes and Hughes [200] discovered the fascinating ‘non-Hermitian Anderson skin effect’ (NHASE) in the Hatano-Nelson model where a non-Hermitian system initially exhibiting no skin effect develops an NHSE under the effect of disorder which is accompanied by a transition in the winding number to non-zero values. Sarkar *et al.* [218] discovered a similar NHASE in the non-Hermitian SSH model and investigated the role of different non-Hermitian symmetries in this context. Interestingly, the NHASE occurs under disorder in symmetry classes A, AIII and D^\dagger . Notably, however, only when all the symmetries of the system are broken does the real space winding number show a direct correspondence to the NHASE.

There have also been recent studies of disorder in non-Hermitian systems using field theoretical tools [219] and transfer matrix calculations [220]. Wanjura *et al.* [221] discovered that non-Hermitian systems can exhibit directional amplification even in the presence of complex (local or non-local) disorder, as long as the size of the point gap in the spectrum remains larger than the maximum disorder introduced into the system. Further, Ref. [197] reported the effect of disorder on higher-order NHSE. Recently, Okuma and Sato [222] have generalized the concept of NHSE to Hermitian disordered systems via the Green’s function approach, where a Hermitian Hamiltonian modified by its self-energy effectively acts as a non-Hermitian one.

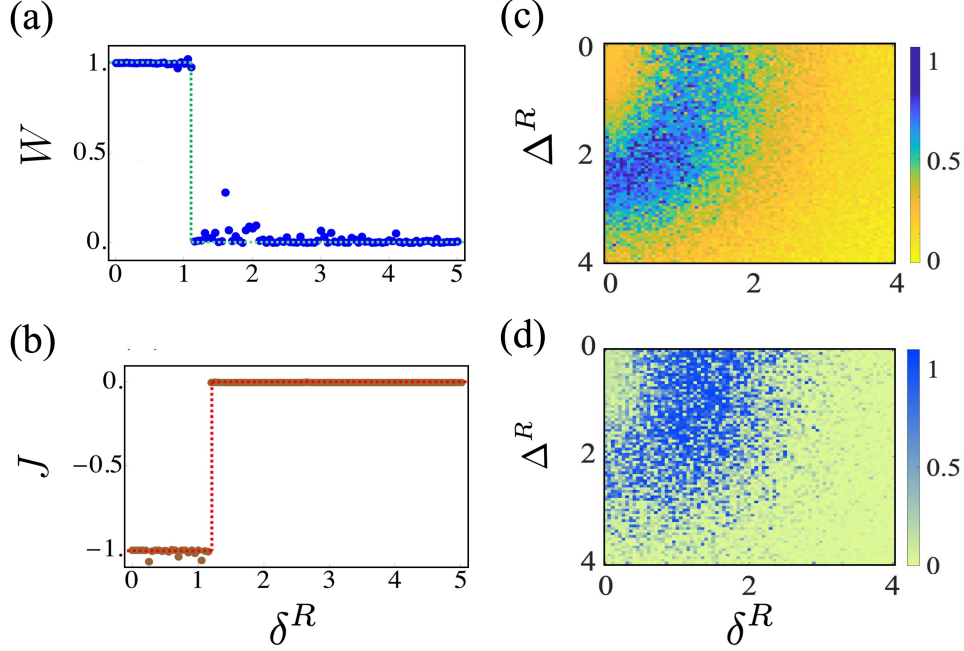


FIG. 8. Equivalence between the current and the winding number under disorder and disorder induced NHASE. (a) The winding number, W , as a function of disorder under PBC. (b) The chiral current as a function of the same hopping disorder. (a) and (b) show that the winding number and chiral current are equivalent, both showing quantized and robust behaviour under disorder. Panel (c) shows the NHASE where a non-Hermitian skin effect develops in the system under disorder when one starts from a set of parameters without skin effect. Here the colour plot denotes the edge density as a function of both hopping disorder and onsite disorder. Panel (d) shows the real space winding number for the system with all broken symmetries demonstrating a correspondence with the edge density under the broken symmetry condition. For (a) and (b) $t_1 = 1.0$, $t_2 = 1.0$, and $\delta = 0.3$, whereas, for (c) and (d) $t_1 = 1.1$, $t_2 = 1.0$, and $\delta = 2.1$. For all plots, we use 400 lattice sites and $\gamma = 0$.

As an illustration of the interesting effects of disorder (adapted from our previous work [218]), we consider the non-Hermitian SSH model with nearest neighbour couplings, non-reciprocal intracell hopping and complex onsite potentials. Disorder is introduced into the system via the non-reciprocity parameter (δ) and the on-site energies (γ). Each non-reciprocal hopping in the real space becomes $\delta_i = \delta + \delta_i^R$ where each $\delta_i^R \in \delta^R[-1, 1]$. Here, δ is the mean value about which disorder of strength δ^R is added. A similar set of random values is added to the on-site gain and loss terms $\gamma_i = \gamma + \Delta_i^R$ where $\Delta_i^R \in \Delta^R[-1, 1]$ and

the disorder strength is denoted by Δ^R . We compute the real space winding number and the current (given in Eq. 24) as a function of increasing disorder. In order to calculate the real space winding number we define a base energy, E_b and construct the matrix $H - E_b I$. On performing a singular value decomposition, we obtain the form $H - E_b I = MSN^\dagger$, where S is a diagonal matrix with eigenvalues along the diagonal. Then, one can define $Q = MN^\dagger$ and $P = NSN^\dagger$, such that $H - E_b I = QP$. From this polar decomposed form of the Hamiltonian we can write

$$W = \frac{1}{L'} \text{Tr}'(Q^\dagger[Q, X]). \quad (30)$$

Here X is the position operator. The trace is taken only over the bulk of the system so a sufficient number of lattice sites is eliminated from both edges. The effective bulk length is $L' = L - 2l$, where L is the total length of the lattice while l is a cutoff length.

As shown in Fig. 8, plotting W and J with respect to the disorder strength values, we find that there is an exact equivalence between the winding number and the current. Interestingly, the current shows a robust and quantized behaviour retaining its clean system value till it makes a sharp transition and drops to zero exactly where the winding number too becomes trivial. Fig. 8 (a) and (b) are shown for disorder in δ however, qualitatively the same behaviour is obtained for disorder in the onsite energies [178]. In Fig. 8 (c), we illustrate the NHASE in the same system. Starting from a region with no skin effect, increasing either kind of disorder (δ^R or Δ^R) or both, the system develops a skin effect (shown by a large increase in edge density) dubbed the NHASE. The edge density is calculated as the local density of states at the edge of the system given by $\frac{\sum_{x_i=1}^{x_E} |\psi_\alpha(x_i)|^2}{\sum_{x_i} |\psi_\alpha(x_i)|^2}$, where x_E denotes the width of the edge. As mentioned in the previous discussion, the NHASE occurs for several symmetry classes. However, when all the symmetries of the system are broken, the real space winding number shows an exact equivalence to the NHASE (as shown in Fig. 8(d)).

IX. NON-HERMITIAN LINEAR RESPONSE THEORY

With growing progress in the understanding of non-Hermitian systems, it has become important to understand how they respond to external perturbations. This has necessitated the development of new paradigms, which we discuss next. Linear response theory has been widely used to study the response of a system under the influence of an external

source [223–225]. When the effect of this external source acts as a small perturbation to a quantum mechanical system, the change in the expectation value of any operator is assumed to be linear in the perturbation

$$\delta\langle O(t)\rangle = \int dt' \chi(t, t') \phi_{ext}(t'), \quad (31)$$

where $\chi(t, t')$ is known as the response function, $\delta\langle O(t)\rangle$ is the change in the expectation value of an operator and $\phi_{ext}(t)$ is the external perturbation acting on the system. With the help of the linear response theory, one can study electrical transport through the Kubo formula and fluctuations through the celebrated fluctuation-dissipation theorem on a system and analyze response of systems when coupled with suitable experimental probes [226, 227]. However, these concepts are well-established only in the Hermitian realm. Non-Hermitian physics requires a modified version of the linear response theory.

A vital step in this direction was taken by Pan *et al.*, by developing the non-Hermitian linear response theory [228]. They analyzed the effects of a non-Hermitian perturbation on a Hermitian Hamiltonian. Cold atom setups are useful platforms to realize non-Hermitian systems [145, 229–232]. Therefore, as an application, Pan *et al.* used their theory to study the real-time dynamics of the momentum distribution of a cold-atom setup that realized the dissipative Bose-Hubbard model [228]. According to their prediction, the height and width of the momentum distribution should be controlled by a similar function. Hence, it is not essential to undertake separate measurements for these parameters. They reexamined the experimental data on peak height and width as a function of time together with the function obtained employing non-Hermitian linear response theory. They found that the data points with smaller error bars closely match the predictions from the theory. Furthermore, using this theoretical framework, they successfully evaluated the critical exponent for a quantum system in the critical phase.

Very recently, a generalized framework of linear response theory has been developed for non-Hermitian perturbations on a non-Hermitian system by Striclet *et al.* [233]. Next, we briefly discuss this formalism. In this framework, the change of an operator $A(t)$ of such a system (to linear order) is given by,

$$\delta\langle A(t)\rangle = \frac{\text{tr}[\delta\rho_I(t)A_I(t)]}{\text{tr}[\rho_0(t)]} - \langle A(t)\rangle_0 \frac{\text{tr}[\delta\rho(t)]}{\text{tr}[\rho_0(t)]}, \quad (32)$$

where $\rho_0(t)$ is the density matrix of the unperturbed system and $\delta\rho(t)$ arises due to the perturbation, $\langle A(t) \rangle_0$ is the expectation value determined in the unperturbed system and $\delta\rho_I(t) = e^{iH_0 t/\hbar} \delta\rho(t) e^{-iH_0^\dagger t/\hbar}$ and $A_I(t) = e^{iH_0^\dagger t/\hbar} A e^{-iH_0 t/\hbar}$ are represented in the interaction picture. Here H_0 is the non-Hermitian Hamiltonian of the unperturbed system. We note that the terms in the denominator are required for proper normalization as the unperturbed Hamiltonian is non-Hermitian. Additionally, the second term appears because of the non-unitary dynamics of the non-Hermitian picture as a norm correction term, hence it is absent in Hermitian linear response theory. The generalized response function is found to be

$$\chi_{AB}(t, t') = -\frac{i}{\hbar} \theta(t - t') \text{tr} \left\{ [[A(t - t'), B]_{\sim} - \langle A(t) \rangle_0 [e^{iH_0^\dagger(t-t')/\hbar} e^{-iH_0(t-t')/\hbar}, B]_{\sim}] \cdot \frac{\rho_0(t')}{\text{tr}[\rho_0(t)]} \right\}, \quad (33)$$

where H_0 is the unperturbed non-Hermitian Hamiltonian, B is the operator associated with the external time-dependent perturbation, $[X, Y]_{\sim} = XY - Y^\dagger X$ is the modified commutator. The first term in the response function is the modified Kubo formula for non-Hermitian cases and second term, as mentioned already, is the norm correction term. Using Eq. (33), the standard Kubo formula can be recovered when $H_0 = H_0^\dagger$ and $B = B^\dagger$. Furthermore, one can retrieve the earlier results by Pan *et al.* [228], i.e., the effect of a non-Hermitian perturbation on a Hermitian system, where $H_0 = H_0^\dagger$ but $B \neq B^\dagger$.

Using this theory, Striclet *et al.* [233] showed that a one-dimensional non-Hermitian relativistic Dirac model with a tachyon phase has a finite conductivity, similar to the two-dimensional graphene sheet. The imaginary mass of the particles results in the non-Hermiticity in the model. Further, the expectation values of the current in this model that were determined using linear response theory and from the numerical solution of the Schrödinger equation match very well, away from the EPs. We also note that the experimental measurement of the unequal-time anti-commutators of observables is also made possible by this non-Hermitian linear response theory, which results in the direct verification of the fluctuation-dissipation theorem [234].

X. TRANSPORT SIGNATURES OF NON-HERMITIAN SYSTEMS

As we have learned from Hermitian topological phases, many key topological features manifest in the transport properties of the system. In the last few years, extensive research has been undertaken to understand how the presence of non-Hermiticity modifies the transport phenomena in a non-Hermitian system [78, 235, 236]. Here, we summarize the recent findings about an important transport signature, namely the Hall conductivity of non-Hermitian topological systems.

For the Hermitian two-dimensional Chern insulator, the Chern number associated with the filled bands, determines the number of edge modes of the gapped insulator. The Hall conductance is proportional to the sum of the Chern numbers of all the filled bands given by the Thouless-Kohmoto-Nightingale-den Nijs (TKNN) formula [237]. When the systems come into contact with the environment, the effective Hamiltonian describing the system becomes non-Hermitian. The imaginary term in the Hamiltonian broadens the density-of-states in the band gap in the complex energy plane. If the minimum separation between the real part of the eigenenergies is much larger than the imaginary part, the non-Hermitian bands can be considered to be “gapped”.

Let us now look at the Hall conductivity for a generic non-Hermitian two-band Hamiltonian of the form

$$H(\mathbf{k}) = (d_{\mathbf{k}}^0 - i\Gamma_{\mathbf{k}}^0)\sigma_0 + (\mathbf{d}_{\mathbf{k}} - i\mathbf{\Gamma}_{\mathbf{k}}) \cdot \boldsymbol{\sigma}_{\mathbf{k}}, \quad (34)$$

where $\mathbf{d}_{\mathbf{k}} = (d_{\mathbf{k}}^x, d_{\mathbf{k}}^y, d_{\mathbf{k}}^z)$ and $\mathbf{\Gamma}_{\mathbf{k}} = (\Gamma_{\mathbf{k}}^x, \Gamma_{\mathbf{k}}^y, \Gamma_{\mathbf{k}}^z)$ are the three component vectors. The current-current correlation is given by

$$K_{\alpha\beta}(\omega) = \sum_{\mathbf{k}} \int d\epsilon d\epsilon' \frac{n_F(\epsilon') - n_F(\epsilon)}{\epsilon' - \epsilon + \omega + i0^+} \text{tr}(\hat{J}_{\alpha} A(\epsilon) \hat{J}_{\beta} A(\epsilon')), \quad (35)$$

where $n_F(\epsilon)$ is the Fermi distribution function at temperature T , $\hat{J}_{\alpha,\beta} = \frac{\partial \text{Re} H(\mathbf{k})}{\partial k_{\alpha,\beta}}$ is the current operator, $A(\epsilon) = \text{Im} \text{tr} \hat{G}^R$ is the spectral function, and \hat{G}^R is the retarded Green's function. Then using the linear response theory, the Kubo formula for the Hall conductance of the system is defined as

$$\sigma_{\alpha\beta} = \lim_{\omega \rightarrow 0} \frac{i}{\omega + i0^+} [K_{\alpha\beta}(\omega) - K_{\alpha\beta}(0)]. \quad (36)$$

The zero temperature limit of $\sigma_{\alpha\beta}$ can be obtained as

$$\sigma_{xy} = \sum_{\mathbf{k}} \frac{\Omega_{xy}(\mathbf{k}) + \Omega_{xy}^*(\mathbf{k})}{2} \times \left(\frac{2}{\pi} \arctan \frac{\text{Re } \epsilon(\mathbf{k})}{\text{Im } \epsilon(\mathbf{k})} \right). \quad (37)$$

Here, $\Omega_{xy}(\mathbf{k}) = \mathbf{h}_{\mathbf{k}} \cdot (\partial_{k_x} \mathbf{d}_{\mathbf{k}} \times \partial_{k_y} \mathbf{d}_{\mathbf{k}}) / \epsilon(\mathbf{k})^3$, $\mathbf{h}(\mathbf{k}) = (\mathbf{d}_{\mathbf{k}} - i\Gamma_{\mathbf{k}})$ and $\epsilon(\mathbf{k})$ is the eigenenergy of the Hamiltonian. The presence of the second term is a manifestation of the non-Hermiticity and it can take any value between $[0, 1]$ depending on the strength of the non-Hermitian terms present in the system. Eq. (37) is the non-Hermitian version of the TKNN formula as obtained in Reference [235].

As a concrete illustration, we use the previously discussed Chern insulator model to analyze the Hall conductivity. The Hamiltonian is given by

$$H(\mathbf{k}) = (\sin k_x + i\gamma(\mathbf{k}))\sigma_x + (\sin k_y + i\gamma(\mathbf{k}))\sigma_y + (m + \cos k_x + \cos k_y)\sigma_z. \quad (38)$$

When $\gamma \rightarrow 0$, i.e., in the Hermitian limit, this Hamiltonian describes a Hermitian Chern insulator. For $-1 < m < 0$, $\sigma_H = -1$ and for $0 < m < 1$, $\sigma_H = 1$. For other values of m , we have $\sigma_H = 0$. Here γ can in general, be dependent on momentum, and $|\gamma(\mathbf{k})|$ is always less than unity, such that the imaginary part of the eigenenergies always lie in the negative half of the complex energy plane. Strikingly, even if the non-Hermitian Chern number remains quantized for a “gapped” non-Hermitian insulator, the Hall conductance is no longer a quantized quantity. In Fig. 9(a) the Hall conductance for this non-Hermitian model is plotted as a function of m considering the imaginary terms to be momentum independent. Whenever m lies in between $\pm\gamma$, the deviation from quantization is more substantial. This deviation increases and the Hall conductivity decreases with the increasing strength of γ , as shown in Fig. 9(b). The inset in Figure 9(b) shows that the Hall conductivity for low values of γ varies linearly.

The non-universal deviation of Hall conductance of a lossy Chern insulator from quantization is due to the broadening of the spectral function gap and the decay term present in the energy of the edge modes [235, 238, 239]. In other words, the probability that the carriers will make it to the other end during transport is less than unity. With increasing strength of the imaginary term in the Hamiltonian, the Hall conductance monotonically decreases. Further, it was also noted that the bulk contribution to the Hall conductance of a non-Hermitian Hamiltonian is non-zero [235]. Additionally, a new contribution to the Hall

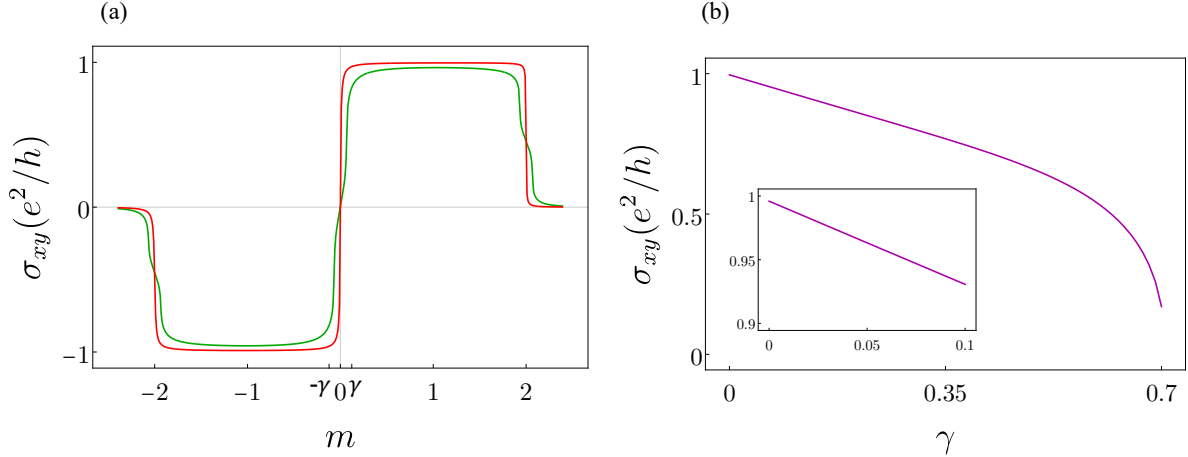


FIG. 9. **Hall conductance of a non-Hermitian Chern insulator.** (a) The Hall conductivity of the non-Hermitian Chern insulator (green curve) is shown along with the Hall conductance of the model in absence of the non-Hermiticity (red curve) as a function of m . Here, γ is taken to be momentum independent and has a numerical value of 0.05. Panel (b) shows the Hall conductivity as a function of the momentum independent non-Hermiticity parameter γ when $m = 1$. The inset shows the linear scaling at small values of γ .

conductance emerges when the system couples to the environment in such a way that the system experiences compensated momentum-independent gain and loss [240]. This universal non-analytic contribution follows a $3/2$ -power law relation with the system parameters (mass term, chemical potential, gain and loss parameter). Very recently, a few theoretical works on Hall conductance in three-dimensional non-Hermitian time-reversal-breaking systems have also appeared [139, 152]. An in-depth understanding of transport properties of such systems will be worth pursuing.

XI. PHYSICAL PLATFORMS AND EXPERIMENTAL ADVANCES

We now present a brief survey of realizations of non-Hermitian Hamiltonians in various physical platforms featuring non-Hermitian topology, which in turn offers intriguing applications and novel functionalities in non-conserving settings. Dissipation and losses are expected in most of the physical systems, however tuning dissipation in a controllable manner leads to wide variety of exotic phenomena with potential applications [19, 20]. Along with delicate theoretical beauty, the application of non-Hermitian topology can be found

in both classical systems, including optical setups with gain and loss [31, 241], electric circuits [139, 242], and quantum systems such as electronic transport setups at material junctions [102, 243], and dissipative cold-atom experiments [86]. The light-matter topological insulator with non-Hermitian topology in photonic crystals holds great promise both for fundamental discoveries and for opening the door to exciting applications in optoelectronics, lasing, as well as transport [236, 244–248].

Recently, the intimate interplay of non-Hermiticity and topological photonics led to the realization of Weyl exceptional rings in an evanescently coupled bipartite optical waveguide array by introducing breaks between waveguides [88]. Combining the ideas of circular modulation of waveguides and insertion of breaks to achieve efficient gain and loss, one can tune non-Hermitian topological semimetals in different dimensions [151]. For an in-depth account of non-Hermitian topological photonics, we refer to the review by Pardo *et al.*, that features various photonic non-Hermitian platforms, EP dynamics, and recent advancements in these growing fields [31]. Mechanical systems such as acoustic materials and metamaterials provide another intriguing prospect for the experimental study of non-Hermitian topological phases. Recently, in the pioneering work of Ghatak *et al.* [249], non-Hermitian topology of the non-reciprocal SSH model has been realized in terms of the dynamical matrix in robotic metamaterials consisting of mechanical rotors, control systems, and springs. These systems manifest non-reciprocal hopping through non-uniform strain in the springs connected to two adjacent rotors. Non-Hermitian topology delineating exceptional structure and concomitant phase transitions in mechanical metamaterials have also been reported in Refs. [250–253]. Interestingly, non-Hermitian chiral active matter systems have also recently emerged as a promising platform to experimentally realize the exceptional edge modes proposed by Sone *et al.* [254].

Electric circuits present another classical platform which enables realization of non-Hermitian topology. In the classical topoelectrical circuit framework, the circuit components, such as periodic arrays of capacitors and inductors, act as Hermitian elements, whereas non-Hermitian effects can be incorporated through dissipative resistance in such arrays. Such topoelectric setups have been shown to simulate diverse phases, and can also be used to readily model various non-Hermitian topological phases [255–261]. For instance, the circuit realization of the non-Hermitian SSH model and the associated skin effect has been reported by Helbig *et al.* [186] and Hofmann *et al.* [188]. Thus, these topoelectrical circuits

serve as a tunable classical platform for theoretical modeling and experimental realization of non-Hermitian topological band structures.

Several ingenious experimental setups have been suggested and realized to engineer EPs in diverse physical platforms. Most notable among them have been in magnetic multilayers [262], waveguides [263, 264], topoelectric circuits [265–267], photonic lattices [31, 244], and topological insulator-ferromagnet junctions [102]. Recent theoretical proposals and experimental demonstrations show that a bulk Fermi arc arises from the topological protection of EPs in an open system of photonic crystal slabs [101]. Interestingly, the bulk Fermi arc is fundamentally different from the conventional surface Fermi arcs that emerge from the two-dimensional projection of Weyl points in three-dimensional Hermitian systems [8]. Furthermore, it leads to fractional topological charge, and the unusual topological band-switching properties across the Fermi arc have also been very recently observed [94, 101, 268]. In addition, the critical behaviour around EPs in the complex parameter space often leads to dramatic effects in a wide range of fields [19, 20], and the theory of EPs has become one of the most exciting emergent front at the crossroads of optics and photonics, acoustics, quantum physics and atomic physics [14, 51, 241, 269–271]. Its explorations have led to many intriguing proposals, such as uni-directional sensitivity [272, 273], band merging [97, 274], laser mode selectivity [270, 275], optomechanical energy transfer [276], and interesting quantum dynamics of exciton-polaritons [277, 278], to name just a few. The EPs in PT -symmetric systems emerge naturally in open quantum platforms owing to a balanced gain and loss interaction between the system and the environment. They result in a wide range of applications, such as single mode coherent lasing [270], negative refraction [279], enhancement of sensing [33, 280] and unidirectional cloaking [281], due to the unique kind of eigenstructures in PT broken and unbroken parameter regimes [244, 246, 282, 283].

An exciting recent experimental development was made in realizing the NHSE in a photonic system by Weidemann *et al.* [180], where non-Hermiticity was invoked by tailoring anisotropy in the nearest-neighbour coupling in an optical fibre. This anisotropy was controlled by amplitude and phase modulators. The authors discovered that when an interface is introduced in the system, all the eigenstates travel towards the interface and localize there, which essentially acts like a “topological funnel” for the light field and demonstrates the NHSE. Further, Zhang *et al.* [183] demonstrated the occurrence of a higher-order NHSE in an acoustic topological insulator where opposite spins can be localized at opposite corners

of the sample by controlling the nature and strength of the non-Hermiticity. Other aspects of NHSE have been recently summarized in Ref. [21]. There exist a few reports of tuning transport in non-Hermitian topological systems. For instance, topologically resilient light can be directed and guided along any arbitrary route thanks to non-Hermitian control in photonic topological insulators [284]. Zhao *et al.* used optical pumping to introduce non-Hermiticity into a coupled microring resonator system, which generated dispersed gain (via external pumping) and loss (intrinsic material loss), and the topological pathways for light were created due to local non-Hermiticity at the boundary of the gain and loss domain. This customizable non-Hermitian topological navigation of light opens up possibilities for high-density data processing in integrated photonic circuitry.

XII. OVERVIEW AND OUTLOOK

In summary, we presented key concepts underlying the physics of non-Hermitian topological phases. By means of concrete, paradigmatic models – Hatano-Nelson, non-Hermitian Su-Schrieffer-Heeger, and non-Hermitian Chern insulator – we illustrated the important features of non-Hermitian topological systems. We summarized the non-Hermitian symmetry classes and discussed the notion of complex energy gaps. We highlighted the non-Hermitian skin effect and the role of generalized Brillouin zone in restoring the bulk-boundary correspondence. We examined the role of disorder and the linear response of such non-Hermitian phases. We also surveyed the rapidly growing experimental advances made in the field.

We would like to end by highlighting here some possible directions which, in our view, may be promising for future explorations. The role of interactions in non-Hermitian topological phases remains to be fully unravelled. While there are a few initial promising studies [169, 285–298], a complete picture is lacking at present. Another important aspect is to understand the time dynamics and steady state nature of such non-Hermitian topological phases and their phase transitions [77, 170, 299–305]. Preliminary investigations have revealed the presence of intriguing non-equilibrium steady state phases that may be characterized by the entanglement properties [63]. The role of dimensionality in this regard may also prove to be important. An open question is the connection between the Liouvilian frameworks, which are well-established for open quantum systems [306], and effective non-Hermitian Hamiltonian approaches, which are predominantly used for non-Hermitian

topological phases. We note that there are a few recent forays into exploring this connection [110, 174, 307–310], although a full understanding is as yet out of reach. Machine learning and artificial intelligence tools are growing in importance in physical sciences [311]. Very recently, there have been a handful of studies using both supervised and unsupervised machine learning approaches to characterize non-Hermitian topological phases [312–316]. Use of such methods to discover and design non-Hermitian systems presents a tantalizing prospect. In conclusion, we are optimistic that many interesting aspects of non-Hermitian topological phases remain to be discovered, and we hope that the present review can help crystallize some of them.

ACKNOWLEDGMENTS

We are grateful to Adhip Agarwala, Arka Bandyopadhyay, Amartya Bose, Nisarg Chadha, Debashree Chowdhury, Tanmoy Das, Suraj Hegde, Rimika Jaiswal, Madhusudan Manjunath, Tobias Meng, Subroto Mukerjee, Brajesh Narayan, Afsar Reja, and Vijay Shenoy for discussions and collaborations. A. B., R. S., and S. D. are supported by the Prime Minister’s Research Fellowship (PMRF). A. N. acknowledges support from the startup grant of the Indian Institute of Science (SG/MHRD-19-0001) and DST-SERB (project number SRG/2020/000153).

-
- [1] P. A. M. Dirac, *The principles of quantum mechanics*, 27 (Oxford university press, 1981).
 - [2] N. Moiseyev, *Non-Hermitian quantum mechanics* (Cambridge University Press, 2011).
 - [3] C. M. Bender and S. Boettcher, Physical review letters **80**, 5243 (1998).
 - [4] C. M. Bender, Reports on Progress in Physics **70**, 947 (2007).
 - [5] M. Stone, *Quantum Hall Effect* (World Scientific, 1992).
 - [6] M. Z. Hasan and C. L. Kane, Reviews of modern physics **82**, 3045 (2010).
 - [7] X.-L. Qi and S.-C. Zhang, Reviews of Modern Physics **83**, 1057 (2011).
 - [8] N. Armitage, E. Mele, and A. Vishwanath, Reviews of Modern Physics **90**, 015001 (2018).
 - [9] B. Lv, T. Qian, and H. Ding, Reviews of Modern Physics **93**, 025002 (2021).
 - [10] B. Yan and S.-C. Zhang, Reports on Progress in Physics **75**, 096501 (2012).

- [11] N. Cooper, J. Dalibard, and I. Spielman, *Reviews of modern physics* **91**, 015005 (2019).
- [12] D.-W. Zhang, Y.-Q. Zhu, Y. Zhao, H. Yan, and S.-L. Zhu, *Advances in Physics* **67**, 253 (2018).
- [13] L. Lu, J. D. Joannopoulos, and M. Soljačić, *Nature photonics* **8**, 821 (2014).
- [14] T. Ozawa, H. M. Price, A. Amo, N. Goldman, M. Hafezi, L. Lu, M. C. Rechtsman, D. Schuster, J. Simon, O. Zilberberg, *et al.*, *Reviews of Modern Physics* **91**, 015006 (2019).
- [15] Y. Liu, X. Chen, and Y. Xu, *Advanced Functional Materials* **30**, 1904784 (2020).
- [16] V. Martinez Alvarez, J. Barrios Vargas, M. Berdakin, and L. Foa Torres, *The European Physical Journal Special Topics* **227**, 1295 (2018).
- [17] A. Ghatak and T. Das, *Journal of Physics: Condensed Matter* **31**, 263001 (2019).
- [18] L. E. F. Torres, *Journal of Physics: Materials* **3**, 014002 (2019).
- [19] Y. Ashida, Z. Gong, and M. Ueda, *Advances in Physics* **69**, 249 (2020).
- [20] E. J. Bergholtz, J. C. Budich, and F. K. Kunst, *Reviews of Modern Physics* **93**, 015005 (2021).
- [21] X. Zhang, T. Zhang, M.-H. Lu, and Y.-F. Chen, *arXiv preprint arXiv:2205.08037* (2022).
- [22] K. Ding, C. Fang, and G. Ma, *Nature Reviews Physics* , 1 (2022).
- [23] T. Kato, *Perturbation theory for linear operators*, Vol. 132 (Springer Science & Business Media, 2013).
- [24] D. C. Brody, *Journal of Physics A: Mathematical and Theoretical* **47**, 035305 (2013).
- [25] I. Rotter, *Journal of Physics A: Mathematical and Theoretical* **42**, 153001 (2009).
- [26] I. Rotter, *Physical Review E* **64**, 036213 (2001).
- [27] W. Heiss, *Journal of Physics A: Mathematical and Theoretical* **45**, 444016 (2012).
- [28] W. D. Heiss, *Journal of Physics A: Mathematical and Theoretical* **41**, 244010 (2008).
- [29] H. Shen, B. Zhen, and L. Fu, *Physical review letters* **120**, 146402 (2018).
- [30] A. Cerjan, M. Xiao, L. Yuan, and S. Fan, *Physical Review B* **97**, 075128 (2018).
- [31] M. Parto, Y. G. Liu, B. Bahari, M. Khajavikhan, and D. N. Christodoulides, *Nanophotonics* **10**, 403 (2021).
- [32] A. Cerjan, A. Raman, and S. Fan, *Physical Review Letters* **116**, 203902 (2016).
- [33] H. Hodaei, A. U. Hassan, S. Wittek, H. Garcia-Gracia, R. El-Ganainy, D. N. Christodoulides, and M. Khajavikhan, *Nature* **548**, 187 (2017).
- [34] R. Jaiswal, A. Banerjee, and A. Narayan, *arXiv preprint arXiv:2107.11649* (2021).

- [35] I. Mandal and E. J. Bergholtz, Physical review letters **127**, 186601 (2021).
- [36] S. Sayyad and F. K. Kunst, arXiv preprint arXiv:2202.07009 (2022).
- [37] P. Delplace, T. Yoshida, and Y. Hatsugai, Physical Review Letters **127**, 186602 (2021).
- [38] D. Heiss, Nature Physics **12**, 823 (2016).
- [39] J.-W. Ryu, S.-Y. Lee, and S. W. Kim, Physical Review A **85**, 042101 (2012).
- [40] L. Gao, Y. Uzun, P. Gao, B. He, X. Ma, J. Wang, S. Han, and K. Tan, “Nature communications 9,” (2018).
- [41] Y. Xiong, Journal of Physics Communications **2**, 035043 (2018).
- [42] Q. Niu, D. J. Thouless, and Y.-S. Wu, Physical Review B **31**, 3372 (1985).
- [43] F. K. Kunst and V. Dwivedi, Physical Review B **99**, 245116 (2019).
- [44] N. Hatano and D. R. Nelson, Physical review letters **77**, 570 (1996).
- [45] N. Hatano and D. R. Nelson, Physical Review B **56**, 8651 (1997).
- [46] J. Y. Lee, J. Ahn, H. Zhou, and A. Vishwanath, Physical Review Letters **123**, 206404 (2019).
- [47] S. Franca, V. Könye, F. Hassler, J. van den Brink, and C. Fulga, Physical Review Letters **129**, 086601 (2022).
- [48] H. Wu, L. Jin, and Z. Song, Physical Review B **103**, 235110 (2021).
- [49] S. Lieu, Physical Review B **97**, 045106 (2018).
- [50] L. Herviou, J. H. Bardarson, and N. Regnault, Physical Review A **99**, 052118 (2019).
- [51] S. Yao and Z. Wang, Physical review letters **121**, 086803 (2018).
- [52] D. Xie, W. Gou, T. Xiao, B. Gadway, and B. Yan, npj Quantum Information **5**, 1 (2019).
- [53] B. Pérez-González, M. Bello, Á. Gómez-León, and G. Platero, arXiv preprint arXiv:1802.03973 (2018).
- [54] Z. Fu, N. Fu, H. Zhang, Z. Wang, D. Zhao, and S. Ke, Applied Sciences **10**, 3425 (2020).
- [55] Y. Zhang, B. Ren, Y. Li, and F. Ye, Optics Express **29**, 42827 (2021).
- [56] L. Li, Z. Xu, and S. Chen, Physical Review B **89**, 085111 (2014).
- [57] H. Schomerus, Optics letters **38**, 1912 (2013).
- [58] M. S. Rudner and L. Levitov, Physical review letters **102**, 065703 (2009).
- [59] Y. Kartik and S. Sarkar, arXiv preprint arXiv:2211.05358 (2022).
- [60] W. Su, J. Schrieffer, and A. J. Heeger, Physical review letters **42**, 1698 (1979).
- [61] J. K. Asbóth, L. Oroszlány, and A. Pályi, Lecture notes in physics **919**, 166 (2016).
- [62] K. Kawabata, T. Bessho, and M. Sato, Physical review letters **123**, 066405 (2019).

- [63] A. Banerjee, S. S. Hegde, A. Agarwala, and A. Narayan, Physical Review B **105**, 205403 (2022).
- [64] K. Kawabata, K. Shiozaki, M. Ueda, and M. Sato, Physical Review X **9**, 041015 (2019).
- [65] T. Yoshida and Y. Hatsugai, Physical Review B **104**, 075106 (2021).
- [66] E. Lee, H. Lee, and B.-J. Yang, Physical Review B **101**, 121109 (2020).
- [67] L. Jin and Z. Song, Physical Review B **99**, 081103 (2019).
- [68] F. K. Kunst, E. Edvardsson, J. C. Budich, and E. J. Bergholtz, Physical review letters **121**, 026808 (2018).
- [69] J. Liu, Y. Han, and C. Liu, Chinese Physics B **28**, 100304 (2019).
- [70] K. Esaki, M. Sato, K. Hasebe, and M. Kohmoto, Physical Review B **84**, 205128 (2011).
- [71] V. M. Alvarez, J. B. Vargas, and L. F. Torres, Physical Review B **97**, 121401 (2018).
- [72] C. Yin, H. Jiang, L. Li, R. Lü, and S. Chen, Physical Review A **97**, 052115 (2018).
- [73] P. St-Jean, V. Goblot, E. Galopin, A. Lemaître, T. Ozawa, L. Le Gratiet, I. Sagnes, J. Bloch, and A. Amo, Nature Photonics **11**, 651 (2017).
- [74] D. S. Borgnia, A. J. Kruchkov, and R.-J. Slager, Physical review letters **124**, 056802 (2020).
- [75] V. M. Vyas and D. Roy, Physical Review B **103**, 075441 (2021).
- [76] Y. He and C.-C. Chien, Journal of Physics: Condensed Matter **33**, 085501 (2020).
- [77] N. Silberstein, J. Behrends, M. Goldstein, and R. Ilan, Physical Review B **102**, 245147 (2020).
- [78] S. Yao, F. Song, and Z. Wang, Physical review letters **121**, 136802 (2018).
- [79] X.-L. Qi, Y.-S. Wu, and S.-C. Zhang, Physical Review B **74**, 085308 (2006).
- [80] T.-D. Lee and C.-N. Yang, Physical Review **87**, 410 (1952).
- [81] H. B. Nielsen and M. Ninomiya, Physics Letters B **130**, 389 (1983).
- [82] S. Murakami, New Journal of Physics **9**, 356 (2007).
- [83] A. Burkov and L. Balents, Physical review letters **107**, 127205 (2011).
- [84] A. Burkov, M. Hook, and L. Balents, Physical Review B **84**, 235126 (2011).
- [85] S. M. Young, S. Zaheer, J. C. Teo, C. L. Kane, E. J. Mele, and A. M. Rappe, Physical review letters **108**, 140405 (2012).
- [86] Y. Xu, S.-T. Wang, and L.-M. Duan, Physical review letters **118**, 045701 (2017).
- [87] T. Yoshida, R. Peters, N. Kawakami, and Y. Hatsugai, Physical Review B **99**, 121101 (2019).

- [88] A. Cerjan, S. Huang, M. Wang, K. P. Chen, Y. Chong, and M. C. Rechtsman, *Nature Photonics* **13**, 623 (2019).
- [89] S. A. A. Ghorashi, T. Li, M. Sato, and T. L. Hughes, *Physical Review B* **104**, L161116 (2021).
- [90] T. Liu, J. J. He, Z. Yang, and F. Nori, *Physical Review Letters* **127**, 196801 (2021).
- [91] W. Rui, M. M. Hirschmann, and A. P. Schnyder, *Physical Review B* **100**, 245116 (2019).
- [92] X. Zhang, K. Ding, X. Zhou, J. Xu, and D. Jin, *Physical Review Letters* **123**, 237202 (2019).
- [93] H. Zhou, J. Y. Lee, S. Liu, and B. Zhen, *Optica* **6**, 190 (2019).
- [94] W. Tang, X. Jiang, K. Ding, Y.-X. Xiao, Z.-Q. Zhang, C. T. Chan, and G. Ma, *Science* **370**, 1077 (2020).
- [95] K. Wang, L. Xiao, J. C. Budich, W. Yi, and P. Xue, *Physical Review Letters* **127**, 026404 (2021).
- [96] P. He, J.-H. Fu, D.-W. Zhang, and S.-L. Zhu, *Physical Review A* **102**, 023308 (2020).
- [97] B. Zhen, C. W. Hsu, Y. Igarashi, L. Lu, I. Kaminer, A. Pick, S.-L. Chua, J. D. Joannopoulos, and M. Soljačić, *Nature* **525**, 354 (2015).
- [98] R. A. Molina and J. González, *Physical review letters* **120**, 146601 (2018).
- [99] K. Moors, A. A. Zyuzin, A. Y. Zyuzin, R. P. Tiwari, and T. L. Schmidt, *Physical Review B* **99**, 041116 (2019).
- [100] R. Okugawa and T. Yokoyama, *Physical Review B* **99**, 041202 (2019).
- [101] H. Zhou, C. Peng, Y. Yoon, C. W. Hsu, K. A. Nelson, L. Fu, J. D. Joannopoulos, M. Soljačić, and B. Zhen, *Science* **359**, 1009 (2018).
- [102] E. J. Bergholtz and J. C. Budich, *Physical Review Research* **1**, 012003 (2019).
- [103] J. C. Budich, J. Carlström, F. K. Kunst, and E. J. Bergholtz, *Physical Review B* **99**, 041406 (2019).
- [104] K. Shiozaki and S. Ono, *Physical Review B* **104**, 035424 (2021).
- [105] S. Sayyad, M. Stalhammar, L. Rodland, and F. K. Kunst, *arXiv preprint arXiv:2204.13945* (2022).
- [106] W. Rui, Z. Zheng, C. Wang, and Z. Wang, *Physical Review Letters* **128**, 226401 (2022).
- [107] V. Kozii and L. Fu, *arXiv preprint arXiv:1708.05841* (2017).
- [108] Z. Zhang, Z. Yang, and J. Hu, *Physical Review B* **102**, 045412 (2020).
- [109] E. Edvardsson, F. K. Kunst, and E. J. Bergholtz, *Physical Review B* **99**, 081302 (2019).

- [110] F. Song, S. Yao, and Z. Wang, Physical review letters **123**, 246801 (2019).
- [111] H. Wang, J. Ruan, and H. Zhang, Physical Review B **99**, 075130 (2019).
- [112] A. Banerjee and A. Narayan, Journal of Physics: Condensed Matter **33**, 225401 (2021).
- [113] X. Yang, Y. Cao, and Y. Zhai, Chinese Physics B **31**, 010308 (2022).
- [114] X.-Q. Sun, B. Lian, and S.-C. Zhang, Physical review letters **119**, 147001 (2017).
- [115] B. Lian and S.-C. Zhang, Physical Review B **94**, 041105 (2016).
- [116] W. Chen, H.-Z. Lu, and J.-M. Hou, Physical Review B **96**, 041102 (2017).
- [117] Z. Yan, R. Bi, H. Shen, L. Lu, S.-C. Zhang, and Z. Wang, Physical Review B **96**, 041103 (2017).
- [118] P.-Y. Chang and C.-H. Yee, Physical Review B **96**, 081114 (2017).
- [119] M. Ezawa, Physical Review B **96**, 041202 (2017).
- [120] G. Chang, S.-Y. Xu, X. Zhou, S.-M. Huang, B. Singh, B. Wang, I. Belopolski, J. Yin, S. Zhang, A. Bansil, *et al.*, Physical review letters **119**, 156401 (2017).
- [121] Y. Zhou, F. Xiong, X. Wan, and J. An, Physical Review B **97**, 155140 (2018).
- [122] R. Bi, Z. Yan, L. Lu, and Z. Wang, Physical Review B **96**, 201305 (2017).
- [123] Z. Yang and J. Hu, Physical Review B **99**, 081102 (2019).
- [124] Z. Yang, C.-K. Chiu, C. Fang, and J. Hu, Physical Review Letters **124**, 186402 (2020).
- [125] J. Carlström, M. Stålhammar, J. C. Budich, and E. J. Bergholtz, Physical Review B **99**, 161115 (2019).
- [126] J. Carlström and E. J. Bergholtz, Physical Review A **98**, 042114 (2018).
- [127] H. Hu and E. Zhao, Physical Review Letters **126**, 010401 (2021).
- [128] X. Zhang, G. Li, Y. Liu, T. Tai, R. Thomale, and C. H. Lee, Communications Physics **4**, 1 (2021).
- [129] T. Kitagawa, T. Oka, A. Brataas, L. Fu, and E. Demler, Physical Review B **84**, 235108 (2011).
- [130] A. Narayan, Physical Review B **91**, 205445 (2015).
- [131] Z. Yan and Z. Wang, Physical review letters **117**, 087402 (2016).
- [132] A. Narayan, Physical Review B **94**, 041409 (2016).
- [133] J. Toudert and R. Serna, Optical Materials Express **7**, 2299 (2017).
- [134] H. Hübener, M. A. Sentef, U. De Giovannini, A. F. Kemper, and A. Rubio, Nature communications **8**, 1 (2017).

- [135] Y. Xu, G. Jiang, I. Miotkowski, R. R. Biswas, and Y. P. Chen, Physical review letters **123**, 207701 (2019).
- [136] R. Jaiswal and A. Narayan, Physical Review B **102**, 245416 (2020).
- [137] C. Bao, P. Tang, D. Sun, and S. Zhou, Nature Reviews Physics **4**, 33 (2022).
- [138] L. Li, C. H. Lee, and J. Gong, Physical review letters **121**, 036401 (2018).
- [139] H. Wu and J.-H. An, Physical Review B **105**, L121113 (2022).
- [140] L. He, Z. Addison, J. Jin, E. J. Mele, S. G. Johnson, and B. Zhen, Nature communications **10**, 1 (2019).
- [141] L. Zhou, Physical Review Research **3**, 033184 (2021).
- [142] L. Zhou, R. W. Bomantara, and S. Wu, arXiv preprint arXiv:2203.09838 (2022).
- [143] L. Zhou and W. Han, Physical Review B **106**, 054307 (2022).
- [144] T. Banerjee and K. Sengupta, arXiv preprint arXiv:2209.12939 (2022).
- [145] L. Li, C. H. Lee, and J. Gong, Physical review letters **124**, 250402 (2020).
- [146] D. Chowdhury, A. Banerjee, and A. Narayan, Physical Review B **105**, 075133 (2022).
- [147] A. A. Zyuzin and A. Y. Zyuzin, Physical Review B **97**, 041203 (2018).
- [148] J. Hou, Y.-J. Wu, and C. Zhang, Physical Review A **103**, 033305 (2021).
- [149] T. Oka and S. Kitamura, Annual Review of Condensed Matter Physics **10**, 387 (2019).
- [150] T. Oka and H. Aoki, Physical Review B **79**, 081406 (2009).
- [151] A. Banerjee and A. Narayan, Physical Review B **102**, 205423 (2020).
- [152] P. He and Z.-H. Huang, Physical Review A **102**, 062201 (2020).
- [153] D. Chowdhury, A. Banerjee, and A. Narayan, Physical Review A **103**, L051101 (2021).
- [154] H. Wu, B.-Q. Wang, and J.-H. An, Physical Review B **103**, L041115 (2021).
- [155] X.-W. Luo and C. Zhang, Physical review letters **123**, 073601 (2019).
- [156] A. K. Ghosh and T. Nag, arXiv preprint arXiv:2205.09915 (2022).
- [157] D.-W. Zhang, L.-Z. Tang, L.-J. Lang, H. Yan, and S.-L. Zhu, Science China Physics, Mechanics & Astronomy **63**, 1 (2020).
- [158] A. Altland and M. R. Zirnbauer, Physical Review B **55**, 1142 (1997).
- [159] X. Luo, Z. Xiao, K. Kawabata, T. Ohtsuki, and R. Shindou, Physical Review Research **4**, L022035 (2022).
- [160] R. Hamazaki, K. Kawabata, N. Kura, and M. Ueda, Physical Review Research **2**, 023286 (2020).

- [161] Z. Gong, Y. Ashida, K. Kawabata, K. Takasan, S. Higashikawa, and M. Ueda, *Physical Review X* **8**, 031079 (2018).
- [162] P. M. Vecsei, M. M. Denner, T. Neupert, and F. Schindler, *Physical Review B* **103**, L201114 (2021).
- [163] C.-H. Liu, H. Hu, and S. Chen, *Physical Review B* **105**, 214305 (2022).
- [164] S. Lieu, *Physical Review B* **100**, 085110 (2019).
- [165] H. Zhou and J. Y. Lee, *Physical Review B* **99**, 235112 (2019).
- [166] C.-H. Liu and S. Chen, *Physical Review B* **100**, 144106 (2019).
- [167] S. Weimann, M. Kremer, Y. Plotnik, Y. Lumer, S. Nolte, K. G. Makris, M. Segev, M. C. Rechtsman, and A. Szameit, *Nature materials* **16**, 433 (2017).
- [168] J. Zhong, K. Wang, Y. Park, V. Asadchy, C. C. Wojcik, A. Dutt, and S. Fan, *Physical Review B* **104**, 125416 (2021).
- [169] T. Yoshida and Y. Hatsugai, *arXiv preprint arXiv:2205.09333* (2022).
- [170] S. Longhi, *Physical Review Research* **1**, 023013 (2019).
- [171] L. Li, C. H. Lee, S. Mu, and J. Gong, *Nature communications* **11**, 1 (2020).
- [172] K. Kawabata, M. Sato, and K. Shiozaki, *Physical Review B* **102**, 205118 (2020).
- [173] K. Yokomizo and S. Murakami, *Physical Review B* **104**, 165117 (2021).
- [174] S. Longhi, *Physical Review B* **102**, 201103 (2020).
- [175] S. Longhi, *Physical Review B* **104**, 125109 (2021).
- [176] J. Zhong, K. Wang, Y. Park, V. Asadchy, C. C. Wojcik, A. Dutt, and S. Fan, *Phys. Rev. B* **104**, 125416 (2021).
- [177] Y. Song, W. Liu, L. Zheng, Y. Zhang, B. Wang, and P. Lu, *Physical Review Applied* **14**, 064076 (2020).
- [178] R. Sarkar, A. Bandyopadhyay, and A. Narayan, *arXiv preprint arXiv:2207.14612* (2022).
- [179] X.-Q. Sun, P. Zhu, and T. L. Hughes, *Physical review letters* **127**, 066401 (2021).
- [180] S. Weidemann, M. Kremer, T. Helbig, T. Hofmann, A. Stegmaier, M. Greiter, R. Thomale, and A. Szameit, *Science* **368**, 311 (2020).
- [181] X. Zhu, H. Wang, S. K. Gupta, H. Zhang, B. Xie, M. Lu, and Y. Chen, *Physical Review Research* **2**, 013280 (2020).
- [182] Z. Fang, M. Hu, L. Zhou, and K. Ding, *arXiv preprint arXiv:2204.08866* (2022).

- [183] X. Zhang, Y. Tian, J.-H. Jiang, M.-H. Lu, and Y.-F. Chen, *Nature communications* **12**, 1 (2021).
- [184] S. Puri, J. Ferdous, A. Shakeri, A. Basiri, M. Dubois, and H. Ramezani, *Physical Review Applied* **16**, 014012 (2021).
- [185] D. Zou, T. Chen, W. He, J. Bao, C. H. Lee, H. Sun, and X. Zhang, *Nature Communications* **12**, 1 (2021).
- [186] T. Helbig, T. Hofmann, S. Imhof, M. Abdelghany, T. Kiessling, L. Molenkamp, C. Lee, A. Szameit, M. Greiter, and R. Thomale, *Nature Physics* **16**, 747 (2020).
- [187] T. Yoshida, T. Mizoguchi, and Y. Hatsugai, *Physical Review Research* **2**, 022062 (2020).
- [188] T. Hofmann, T. Helbig, F. Schindler, N. Salgo, M. Brzezińska, M. Greiter, T. Kiessling, D. Wolf, A. Vollhardt, A. Kabaši, *et al.*, *Physical Review Research* **2**, 023265 (2020).
- [189] D.-A. Galeano, X.-X. Zhang, and J. Mahecha, *Science China Physics, Mechanics & Astronomy* **65**, 1 (2022).
- [190] K. Zhang, Z. Yang, and C. Fang, *Physical Review Letters* **125**, 126402 (2020).
- [191] N. Okuma, K. Kawabata, K. Shiozaki, and M. Sato, *Physical review letters* **124**, 086801 (2020).
- [192] K. Zhang, Z. Yang, and C. Fang, *Nature communications* **13**, 1 (2022).
- [193] R. Okugawa, R. Takahashi, and K. Yokomizo, *Physical Review B* **102**, 241202 (2020).
- [194] M. Lu, X.-X. Zhang, and M. Franz, *Physical review letters* **127**, 256402 (2021).
- [195] K. Kawabata, N. Okuma, and M. Sato, *arXiv preprint arXiv:2003.07597* (2020).
- [196] K. Yokomizo and S. Murakami, *Physical review letters* **123**, 066404 (2019).
- [197] K.-M. Kim and M. J. Park, *Physical Review B* **104**, L121101 (2021).
- [198] Q.-B. Zeng and Y. Xu, *Physical Review Research* **2**, 033052 (2020).
- [199] S. Longhi, *Physical Review B* **103**, 144202 (2021).
- [200] J. Claes and T. L. Hughes, *Physical Review B* **103**, L140201 (2021).
- [201] H. Liu, J.-K. Zhou, B.-L. Wu, Z.-Q. Zhang, and H. Jiang, *arXiv preprint arXiv:2102.12189* (2021).
- [202] H. Liu, M. Lu, Z.-Q. Zhang, and H. Jiang, *arXiv preprint arXiv:2208.03013* (2022).
- [203] Z.-Q. Zhang, H. Liu, H. Liu, H. Jiang, and X. Xie, *arXiv preprint arXiv:2201.01577* (2022).
- [204] I. Mondragon-Shem, T. L. Hughes, J. Song, and E. Prodan, *Physical review letters* **113**, 046802 (2014).

- [205] R. Wang, K. Zhang, and Z. Song, *Journal of Physics Communications* **5**, 095011 (2021).
- [206] C. Zhang, L. Sheng, and D. Xing, *Physical Review B* **103**, 224207 (2021).
- [207] J. Claes and T. L. Hughes, *Physical Review B* **101**, 224201 (2020).
- [208] A. Tzortzakakis, K. Makris, and E. Economou, *Physical Review B* **101**, 014202 (2020).
- [209] Y. Huang and B. I. Shklovskii, *Physical Review B* **101**, 014204 (2020).
- [210] X. Luo, T. Ohtsuki, and R. Shindou, *Physical Review Letters* **126**, 090402 (2021).
- [211] Y. Huang and B. I. Shklovskii, *Physical Review B* **102**, 064212 (2020).
- [212] H. Jiang, L.-J. Lang, C. Yang, S.-L. Zhu, and S. Chen, *Physical Review B* **100**, 054301 (2019).
- [213] Y. Liu, Q. Zhou, and S. Chen, *Physical Review B* **104**, 024201 (2021).
- [214] R. Hamazaki, K. Kawabata, and M. Ueda, *Physical review letters* **123**, 090603 (2019).
- [215] X.-W. Luo and C. Zhang, *arXiv preprint arXiv:1912.10652* (2019).
- [216] H. Liu, Z. Su, Z.-Q. Zhang, and H. Jiang, *Chinese Physics B* **29**, 050502 (2020).
- [217] L.-Z. Tang, L.-F. Zhang, G.-Q. Zhang, and D.-W. Zhang, *Physical Review A* **101**, 063612 (2020).
- [218] R. Sarkar, S. S. Hegde, and A. Narayan, *arXiv preprint arXiv:2205.15828* (2022).
- [219] A. Moustaj, L. Eek, and C. M. Smith, *Physical Review B* **105**, L180503 (2022).
- [220] X. Luo, T. Ohtsuki, and R. Shindou, *Physical Review B* **104**, 104203 (2021).
- [221] C. C. Wanjura, M. Brunelli, and A. Nunnenkamp, *Physical Review Letters* **127**, 213601 (2021).
- [222] N. Okuma and M. Sato, *Physical Review Letters* **126**, 176601 (2021).
- [223] A. L. Fetter and J. D. Walecka, *Quantum theory of many-particle systems* (Courier Corporation, 2012).
- [224] D. Pines, *Theory of Quantum Liquids: Normal Fermi Liquids* (CRC Press, 2018).
- [225] G. Giuliani and G. Vignale, *Quantum theory of the electron liquid* (Cambridge university press, 2005).
- [226] D.-n. Shi, M.-w. Xiao, and Z.-z. Li, *Physical Review B* **58**, 12478 (1998).
- [227] A. Tokuno and T. Giamarchi, *Physical review letters* **106**, 205301 (2011).
- [228] L. Pan, X. Chen, Y. Chen, and H. Zhai, *Nature Physics* **16**, 767 (2020).
- [229] M. Kreibich, J. Main, H. Cartarius, and G. Wunner, *Physical Review A* **90**, 033630 (2014).

- [230] J. Li, A. K. Harter, J. Liu, L. de Melo, Y. N. Joglekar, and L. Luo, *Nature communications* **10**, 1 (2019).
- [231] Q. Liang, D. Xie, Z. Dong, H. Li, H. Li, B. Gadway, W. Yi, and B. Yan, *arXiv preprint arXiv:2201.09478* (2022).
- [232] K. Li and Y. Xu, *arXiv preprint arXiv:2201.09469* (2022).
- [233] D. Sticlet, B. Dóra, and C. P. Moca, *Physical Review Letters* **128**, 016802 (2022).
- [234] K. T. Geier and P. Hauke, *PRX Quantum* **3**, 030308 (2022).
- [235] Y. Chen and H. Zhai, *Physical Review B* **98**, 245130 (2018).
- [236] S. Longhi, D. Gatti, and G. D. Valle, *Scientific reports* **5**, 1 (2015).
- [237] D. J. Thouless, M. Kohmoto, M. P. Nightingale, and M. den Nijs, *Physical review letters* **49**, 405 (1982).
- [238] T. M. Philip, M. R. Hirsbrunner, and M. J. Gilbert, *Physical Review B* **98**, 155430 (2018).
- [239] J. Wang, F. Li, and X. Yi, *Chinese Physics B* (2022).
- [240] S. Groenendijk, T. L. Schmidt, and T. Meng, *Physical Review Research* **3**, 023001 (2021).
- [241] B. Midya, H. Zhao, and L. Feng, *Nature communications* **9**, 1 (2018).
- [242] N. K. Gupta and A. M. Jayannavar, *arXiv preprint arXiv:2108.11587* (2021).
- [243] H. C. Park, J.-W. Ryu, and N. Myoung, *Journal of Low Temperature Physics* **191**, 49 (2018).
- [244] L. Feng, R. El-Ganainy, and L. Ge, *Nature Photonics* **11**, 752 (2017).
- [245] R. El-Ganainy, M. Khajavikhan, D. N. Christodoulides, and S. K. Ozdemir, *Communications Physics* **2**, 1 (2019).
- [246] S. Longhi, *EPL (Europhysics Letters)* **120**, 64001 (2018).
- [247] H. Wang, X. Zhang, J. Hua, D. Lei, M. Lu, and Y. Chen, *Journal of Optics* **23**, 123001 (2021).
- [248] M. De Carlo, F. De Leonardis, R. A. Soref, L. Colatorti, and V. M. Passaro, *Sensors* **22**, 3977 (2022).
- [249] A. Ghatak, M. Brandenbourger, J. Van Wezel, and C. Coulais, *Proceedings of the National Academy of Sciences* **117**, 29561 (2020).
- [250] D. Zhou and J. Zhang, *Physical Review Research* **2**, 023173 (2020).
- [251] C. Scheibner, W. T. Irvine, and V. Vitelli, *Physical Review Letters* **125**, 118001 (2020).
- [252] T. Yoshida and Y. Hatsugai, *Physical Review B* **100**, 054109 (2019).

- [253] M. Brandenbourger, X. Locsin, E. Lerner, and C. Coulais, *Nature communications* **10**, 1 (2019).
- [254] K. Sone, Y. Ashida, and T. Sagawa, *Nature communications* **11**, 1 (2020).
- [255] V. V. Albert, L. I. Glazman, and L. Jiang, *Physical review letters* **114**, 173902 (2015).
- [256] J. Ningyuan, C. Owens, A. Sommer, D. Schuster, and J. Simon, *Physical Review X* **5**, 021031 (2015).
- [257] S. Imhof, C. Berger, F. Bayer, J. Brehm, L. W. Molenkamp, T. Kiessling, F. Schindler, C. H. Lee, M. Greiter, T. Neupert, *et al.*, *Nature Physics* **14**, 925 (2018).
- [258] X.-X. Zhang and M. Franz, *Physical Review Letters* **124**, 046401 (2020).
- [259] K. Luo, J. Feng, Y. Zhao, and R. Yu, arXiv preprint arXiv:1810.09231 (2018).
- [260] M. Ezawa, *Physical Review B* **99**, 121411 (2019).
- [261] M. Ezawa, *Physical Review B* **99**, 201411 (2019).
- [262] T. Yu, H. Yang, L. Song, P. Yan, and Y. Cao, *Physical Review B* **101**, 144414 (2020).
- [263] Q. Zhong, A. Ahmed, J. Dadap, R. Osgood Jr, and R. El-Ganainy, *New Journal of Physics* **18**, 125006 (2016).
- [264] X.-L. Zhang and C. T. Chan, *Communications Physics* **2**, 1 (2019).
- [265] J. Schindler, A. Li, M. C. Zheng, F. M. Ellis, and T. Kottos, *Physical Review A* **84**, 040101 (2011).
- [266] A. Stegmaier, S. Imhof, T. Helbig, T. Hofmann, C. H. Lee, M. Kremer, A. Fritzsche, T. Feichtner, S. Klemmt, S. Höfling, *et al.*, *Physical Review Letters* **126**, 215302 (2021).
- [267] Z. Xiao, H. Li, T. Kottos, and A. Alù, *Physical Review Letters* **123**, 213901 (2019).
- [268] R. Su, E. Estrecho, D. Biegańska, Y. Huang, M. Wurdack, M. Pieczarka, A. G. Truscott, T. C. Liew, E. A. Ostrovskaya, and Q. Xiong, *Science advances* **7**, eabj8905 (2021).
- [269] Z. Zhang, Y. Zhang, J. Sheng, L. Yang, M.-A. Miri, D. N. Christodoulides, B. He, Y. Zhang, and M. Xiao, *Physical review letters* **117**, 123601 (2016).
- [270] L. Feng, Z. J. Wong, R.-M. Ma, Y. Wang, and X. Zhang, *Science* **346**, 972 (2014).
- [271] C. Shi, M. Dubois, Y. Chen, L. Cheng, H. Ramezani, Y. Wang, and X. Zhang, *Nature communications* **7**, 1 (2016).
- [272] Z. Lin, H. Ramezani, T. Eichelkraut, T. Kottos, H. Cao, and D. N. Christodoulides, *Physical Review Letters* **106**, 213901 (2011).

- [273] B. Peng, Ş. K. Özdemir, F. Lei, F. Monifi, M. Gianfreda, G. L. Long, S. Fan, F. Nori, C. M. Bender, and L. Yang, *Nature Physics* **10**, 394 (2014).
- [274] K. G. Makris, R. El-Ganainy, D. Christodoulides, and Z. H. Musslimani, *Physical Review Letters* **100**, 103904 (2008).
- [275] H. Hodaei, M.-A. Miri, M. Heinrich, D. N. Christodoulides, and M. Khajavikhan, *Science* **346**, 975 (2014).
- [276] H. Xu, D. Mason, L. Jiang, and J. Harris, *Nature* **537**, 80 (2016).
- [277] T. Gao, G. Li, E. Estrecho, T. Liew, D. Comber-Todd, A. Nalitov, M. Steger, K. West, L. Pfeiffer, D. Snoke, *et al.*, *Physical review letters* **120**, 065301 (2018).
- [278] T. Gao, E. Estrecho, K. Bliokh, T. Liew, M. Fraser, S. Brodbeck, M. Kamp, C. Schneider, S. Höfling, Y. Yamamoto, *et al.*, *Nature* **526**, 554 (2015).
- [279] R. Fleury, D. L. Sounas, and A. Alu, *Physical review letters* **113**, 023903 (2014).
- [280] J. Wiersig, *Nature communications* **11**, 1 (2020).
- [281] D. L. Sounas, R. Fleury, and A. Alù, *Physical Review Applied* **4**, 014005 (2015).
- [282] A. A. Zyablovsky, A. P. Vinogradov, A. A. Pukhov, A. V. Dorofeenko, and A. A. Lisyansky, *Physics-Uspekhi* **57**, 1063 (2014).
- [283] M.-A. Miri and A. Alù, *Science* **363**, eaar7709 (2019).
- [284] H. Zhao, X. Qiao, T. Wu, B. Midya, S. Longhi, and L. Feng, *Science* **365**, 1163 (2019).
- [285] K. Kawabata, K. Shiozaki, and S. Ryu, *Physical Review B* **105**, 165137 (2022).
- [286] T. Hyart and J. L. Lado, *Physical Review Research* **4**, L012006 (2022).
- [287] G. Chen, F. Song, and J. L. Lado, *arXiv preprint arXiv:2208.06425* (2022).
- [288] K. Suthar, Y.-C. Wang, Y.-P. Huang, H. Jen, and J.-S. You, *Physical Review B* **106**, 064208 (2022).
- [289] S. Ghosh, S. Gupta, and M. Kulkarni, *Physical Review B* **106**, 134202 (2022).
- [290] W. N. Faugno and T. Ozawa, *Physical Review Letters* **129**, 180401 (2022).
- [291] T. Yoshida and Y. Hatsugai, *arXiv preprint arXiv:2211.08895* (2022).
- [292] T. Yoshida, R. Peters, and N. Kawakami, *Physical Review B* **98**, 035141 (2018).
- [293] L. Crippa, J. C. Budich, and G. Sangiovanni, *Physical Review B* **104**, L121109 (2021).
- [294] R. Schäfer, J. C. Budich, and D. J. Luitz, *arXiv preprint arXiv:2204.05340* (2022).
- [295] R. Shen and C. H. Lee, *arXiv preprint arXiv:2107.03414* (2021).

- [296] S.-B. Zhang, M. M. Denner, T. Bzdušek, M. A. Sentef, and T. Neupert, arXiv preprint arXiv:2201.12653 (2022).
- [297] S. Sarkar, Scientific Reports **11**, 1 (2021).
- [298] R. R. Kumar, S. Rahul, Y. Kartik, and S. Sarkar, in *Journal of Physics: Conference Series*, Vol. 2038 (IOP Publishing, 2021) p. 012016.
- [299] S. Longhi, Physical Review B **105**, 245143 (2022).
- [300] T. Li, Y.-S. Zhang, and W. Yi, Physical Review B **105**, 125111 (2022).
- [301] L. Zhou, Physical Review B **100**, 184314 (2019).
- [302] C. P. Moca and B. Dóra, Physical Review B **104**, 125124 (2021).
- [303] Y. Pará, G. Palumbo, and T. Macrì, Physical Review B **103**, 155417 (2021).
- [304] S. Longhi, Physical Review Letters **128**, 157601 (2022).
- [305] S. Rahul and S. Sarkar, Scientific Reports **12**, 1 (2022).
- [306] H.-P. Breuer, F. Petruccione, *et al.*, *The theory of open quantum systems* (Oxford University Press, 2002).
- [307] T. Haga, M. Nakagawa, R. Hamazaki, and M. Ueda, Physical Review Letters **127**, 070402 (2021).
- [308] F. Yang, Q.-D. Jiang, and E. J. Bergholtz, Physical Review Research **4**, 023160 (2022).
- [309] C.-H. Liu, K. Zhang, Z. Yang, and S. Chen, arXiv preprint arXiv:2005.02617 (2020).
- [310] Z. Gong and R. Hamazaki, arXiv preprint arXiv:2202.02011 (2022).
- [311] G. Carleo, I. Cirac, K. Cranmer, L. Daudet, M. Schuld, N. Tishby, L. Vogt-Maranto, and L. Zdeborová, Reviews of Modern Physics **91**, 045002 (2019).
- [312] B. Narayan and A. Narayan, Physical Review B **103**, 035413 (2021).
- [313] L.-F. Zhang, L.-Z. Tang, Z.-H. Huang, G.-Q. Zhang, W. Huang, and D.-W. Zhang, Physical Review A **103**, 012419 (2021).
- [314] L.-W. Yu and D.-L. Deng, Physical Review Letters **126**, 240402 (2021).
- [315] H. Araki, T. Yoshida, and Y. Hatsugai, Journal of the Physical Society of Japan **90**, 053703 (2021).
- [316] Y. Yu, L.-W. Yu, W. Zhang, H. Zhang, X. Ouyang, Y. Liu, D.-L. Deng, and L.-M. Duan, arXiv preprint arXiv:2112.13785 (2021).